JBC RESEARCH ARTICLE

A *CACNA1C* variant associated with cardiac arrhythmias provides mechanistic insights in the calmodulation of L-type Ca^{2+} channels

Received for publication, June 12, 2022, and in revised form, October 12, 2022 Published, Papers in Press, October 21, 2022,
https://doi.org/10.1016/j.jbc.2022.102632

Juan Zhao[1,‡], **Emilie Segura**[1,2,‡], **Mireille Marsolais**[1,2], **and Lucie Parent**[1,2,*]

From the [1]*Centre de recherche de l'Institut de Cardiologie de Montréal, Université de Montréal, Montréal, Québec, Canada;* [2]*Département de Pharmacologie et Physiologie, Faculté de Médecine, Montréal, Québec, Canada*

Edited by Mike Shipston

We recently reported the identification of a *de novo* single nucleotide variant in exon 9 of *CACNA1C* associated with prolonged repolarization interval. Recombinant expression of the glycine to arginine variant at position 419 produced a gain in the function of the L-type $Ca_V1.2$ channel with increased peak current density and activation gating but without significant decrease in the inactivation kinetics. We herein reveal that these properties are replicated by overexpressing calmodulin (CaM) with $Ca_V1.2$ WT and are reversed by exposure to the CaM antagonist W-13. Phosphomimetic (T79D or S81D), but not phosphoresistant (T79A or S81A), CaM surrogates reproduced the impact of CaM WT on the function of $Ca_V1.2$ WT. The increased channel activity of $Ca_V1.2$ WT following overexpression of CaM was found to arise in part from enhanced cell surface expression. In contrast, the properties of the variant remained unaffected by any of these treatments. $Ca_V1.2$ substituted with the α-helix breaking proline residue were more reluctant to open than $Ca_V1.2$ WT but were upregulated by phosphomimetic CaM surrogates. Our results indicate that (1) CaM and its phosphomimetic analogs promote a gain in the function of $Ca_V1.2$ and (2) the structural properties of the first intracellular linker of $Ca_V1.2$ contribute to its CaM-induced modulation. We conclude that the *CACNA1C* clinical variant mimics the increased activity associated with the upregulation of $Ca_V1.2$ by Ca^{2+}–CaM, thus maintaining a majority of channels in a constitutively active mode that could ultimately promote ventricular arrhythmias.

Cardiac contraction during the systole is handled by the influx of Ca^{2+} into cardiomyocytes in response to depolarization during phase 2 of the cardiac action potential (1). Voltage-gated L-type calcium channel $Ca_V1.2$ are expressed in the T-tubules such that localized Ca^{2+} entry triggers a sustained and more global Ca^{2+} release by the sarcoplasmic reticulum in the dyadic cleft (2). Cardiac L-type $Ca_V1.2$ channels are hetero-multimeric protein complexes formed by the pore-forming $Ca_V\alpha1C$ subunit bound to the extracellular $Ca_V\alpha2\delta1$ auxiliary subunits (3, 4) and to the cytoplasmic $Ca_V\beta$ (5) that binds with nanomolar affinity to the first intracellular linker (6). The $Ca_V\alpha1$ subunit is formed by a single polypeptide chain of 24 transmembrane helices grouped into four structural homologous domains (domains I, II, II, and IV) (Fig. 1). Although not a specific auxiliary subunit, calmodulin (CaM) contributes to Ca^{2+}-dependent facilitation and Ca^{2+}-dependent inactivation (CDI) of $Ca_V1.2$ (7–9) through binding to the isoleucine–glutamine motif in the C-terminal tail of $Ca_V\alpha1C$ (10–13).

First clinically described in 1957 (14), the long-QT syndrome (LQTS) is a major cause of sudden death in healthy infants and young adults (15–17). Congenital LQTS in the absence of structural defects (18) is often the result of inherited or *de novo* genetic mutations in the DNA of a variety of ion channels (19). Gain-of-function mutations within the *CACNA1C* gene, coding for $Ca_V\alpha1C$, are associated with the LQTS type 8 also referred to as Timothy syndrome (TS) (20–22). Many TS variants were identified in a short region adjoining the sixth transmembrane segment of the $Ca_V\alpha1C$ protein (Fig. 1). The canonical TS1 variant Gly406Arg results from a *de novo CACNA1C* mutation in exon 8A (20). An atypical form of TS type 2 is associated with the Gly402Ser and Gly402Arg variants in the alternatively spliced exon 8 (21). More recent *de novo* mutations have highlighted the importance of this region such as Glu407Gly/Ala (23, 24) and Arg518Cys/His (25). These missense variants are causing a gain of function in the $Ca_V1.2$ channel as a result of slower inactivation kinetics that promote larger Ca^{2+} influx for the same depolarizing pulse (26). Nonetheless, functional outcomes of other TS mutations included marked loss of current density, a gain-of-function shift in activation, and increased window current (27). We have recently identified in the first intracellular region of $Ca_V\alpha1C$ a missense variant, Gly419Arg, from a patient with prolonged QT interval (≈500 ms), syndactyly, left ventricular noncompaction, and slight delay in neurodevelopment (28). Unlike other TS variants located close to the high-affinity binding domain of $Ca_V\beta$, $Ca_V1.2$ Gly419Arg exhibited a gain-of-function shift in the activation gating and no decrease in the channel current decay (28).

Herein, we explored the regulation of the long QTS variant Gly419Arg (G449R in the rabbit clone numbering). Glycine

‡ These authors contributed equally to this work.
* For correspondence: Lucie Parent, lucie.parent@umontreal.ca.

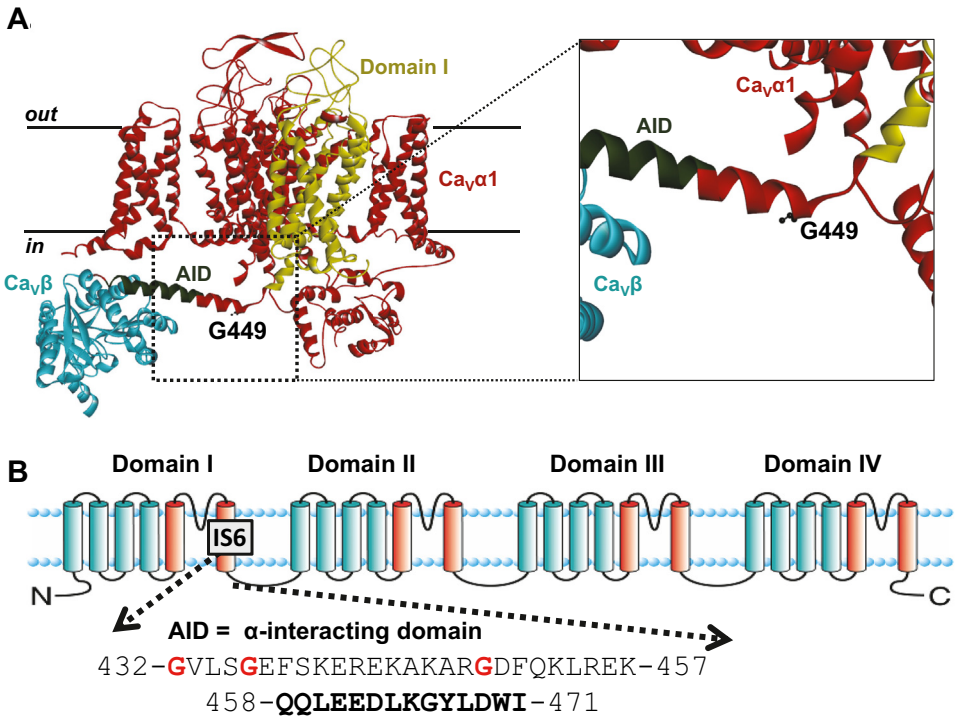

Figure 1. The $Ca_V1.2$ variant is located in the intracellular linker before the binding site for the $Ca_V\beta$ subunit. The LQTS-related $Ca_V\alpha1C$ mutation G449 is located before the α-interacting domain (AID). *A*, the cryo-EM 3D structure of the rabbit $Ca_V1.1$ oligomeric complex at 3.6 Å for $Ca_V\alpha1S$ and at 3.9 Å for $Ca_V\beta$ (Protein Data Bank code: 5GJV). $Ca_V\alpha1C$ and $Ca_V\alpha1S$ share 81% homology in their primary protein sequence. L-type calcium channels share similar structure, being composed of the pore-forming subunit $Ca_V\alpha1$ in *red* and $Ca_V\beta$ in *blue* and an intracellular subunit bound to $Ca_V\alpha1$ through the intracellular helix linking domains I and II of $Ca_V\alpha1$ (shown in *dark green*). The first transmembrane domain of $Ca_V\alpha1$ (DI) is shown in *yellow*. The human LQTS-related $Ca_V\alpha1C$ G419R variant is similar to the rabbit $Ca_V\alpha1C$ G449R and is equivalent to Gly358 in $Ca_V\alpha1S$. Image was produced by Discovery Studio 2020 (BIOVIA Pipeline Pilot 2020). *B*, cartoon of the corresponding secondary structure for the $Ca_V\alpha1C$ pore-forming subunit of the L-type $Ca_V1.2$ channel showing the four homologous domains (domains I to IV) with the N and C termini located into the cytoplasm. The $Ca_V\beta$ subunit–binding site on the $Ca_V\alpha1C$ subunit is referred to the "α-interacting domain" or AID. The AID is located within 20 residues of the sixth transmembrane segment in domain I (IS6). The primary sequence for the AID motif is shown below the primary sequence for the short region extending from the end of S6 to the beginning of the AID. The relative position of three glycine variants reported in the Timothy syndrome (G402S, G406R, and G419R) is fully conserved across species and presented in *red* with the numbering in the rabbit clone used for this study. LQTS, long-QT syndrome.

residues, inserted between the sixth transmembrane segment and the high-affinity binding site for $Ca_V\beta$, have been shown to confer higher flexibility to this region (29–31), leading to reduced basal L-type Ca_V channel activity in cardiomyocytes (30). The reverse proposition, removing or substituting glycine residues in this locus, decreased the linker flexibility (31). Herein, we present evidence that the novel variant, whereby a conserved glycine is substituted by a larger arginine residue, promotes stronger activity (peak current density and activation gating) at physiological voltages akin to a constitutively hyperactive channel. This hyperactive mode was reconstituted in the WT channel by coexpression with CaM WT or pseudo-phosphorylated surrogates CaM T79D or CaM S81D and was abolished by the CaM antagonist W-13. In contrast, the functional parameters of the clinical glycine to arginine variant remained remarkably insensitive to these treatments. Substitution with the α-helix breaker proline residue yielded opposite results with channels more reluctant to open at physiological voltages but more likely to respond to the modulation by CaM. Altogether, the functional characterization of the glycine to arginine variant provides mechanistic insight on the regulation of $Ca_V1.2$ by CaM (sometimes referred to as calmodulation) and specifically the role played by the I–II linker as relaying the signal to the channel activation gate.

Results

Glycine substitution stimulates activation gating and peak current density of $Ca_V1.2$

It is well known that gain-of-function mutations G402S and G406R (Fig. 1) decelerate inactivation kinetics (20, 21, 32–34). In contrast, the inactivation kinetics of the gain-of-function TS $Ca_V1.2$ G419R variant classified as a pathogenic TS variant (35) were slightly faster than $Ca_V1.2$ WT (28). The faster inactivation kinetics were associated with increased peak current density and a leftward shift in the voltage of activation, leading to an increased probability of channel being open at physiological voltages without any significant change in the voltage dependence of inactivation (Table 1). Glycine residues close to the pore (*e.g.*, Gly402 and Gly406) appear to be essential to convey the movement of the inactivation gate, whereas inserting glycine residues further away and closer to the high-affinity binding domain for $Ca_V\beta$ (Fig. 1) yielded opposite results (29, 30). Increased flexibility within this stretch has been argued to loosen up the interaction between

Table 1
Electrophysiological properties of $Ca_V1.2$ WT and G449R with W-13

			Electrophysiological properties				
$Ca_V1.2$	CaM	n/N	Peak I (pA/pF)	$E_{0.5,act}$ (mV)	R100	n/N	$E_{0.5,inact}$ (mV)
WT	Native	30/7	−15 ± 4	−10 ± 3	0.65 ± 0.04	14/5	−33 ± 3
	+W-13	17/4	−8 ± 2 $p = 0.002$ *versus* control	−12 ± 4	0.57 ± 0.02 $p < 0.001$ *versus* control	6/3	−33 ± 3
G449R	Native	31/4	−33 ± 12 $p < 0.001$ *versus* WT	−17 ± 3 $p < 0.001$ *versus* WT	0.52 ± 0.03 $p < 0.001$ *versus* WT	13/4	−35 ± 3
	+W-13	12/1	−38 ± 8	−17 ± 3	0.51 ± 0.03	5/2	−34 ± 2

Effects of CaM inhibitor W-13 on the gating properties of $Ca_V1.2$ WT or G449R channels with native or endogenous CaM. $Ca_V1.2$ WT or G449R were coexpressed in HEKT cells with $Ca_V\beta2a$ and $Ca_V\alpha2\delta1$. Whole-cell currents were measured in the presence of 2 mM Ca^{2+} in the extracellular medium. $E_{0.5,inact}$ values were estimated after a 5 s long depolarizing pulse to 0 mV. Fractional currents were fitted to Boltzmann equations as described in the Experimental procedures section. The R100 values report the relative current decay observed 100 ms after the peak current. n/N refers to the number of cells/transfections measured in each condition of study. Mean ± SD are shown. Statistical analysis was carried out by one-way ANOVA and a Bonferroni post hoc test.

$Ca_V\beta$ and $Ca_V1.2$ (30). We validated that the substitution of the glycine residue at position 449 (rabbit numbering) does not impair the interaction with the canonical $Ca_V\beta$ and $Ca_V\alpha2\delta1$ subunits (Fig. 2). The latter observation is in line with the recent demonstration that interaction with $Ca_V\alpha2\delta1$ involves extracellular loops of $Ca_V1.2$ (4, 36, 37). We thus turned to investigate functional regulation by the ubiquitous CaM (38). Disease-causing mutations at CaM proteins lead to major cardiac dysfunction, and in turn, mutations at the CaM-binding site of ion channels have been associated with a host of diseases (39).

CaM antagonist W-13 blocks $Ca_V1.2$ WT but not G449R whole-cell currents

Functional regulation of $Ca_V1.2$ WT by endogenous CaM was examined with the membrane-permeable naphthalenesulfonamide derivative CaM antagonist W-13. Under our conditions, $Ca_V1.2$ WT currents activated at −35 mV and reached the peak inward current at +5 mV. As seen in Figure 3*A*, the peak current density of $Ca_V1.2$ WT was reduced by about 50% from −15 ± 4 pA/pF to −8 ± 2 pA/pF after adding 10 μM W-13 into the bath. Decay of the $Ca_V1.2$ WT current was accelerated in the presence of W-13, which

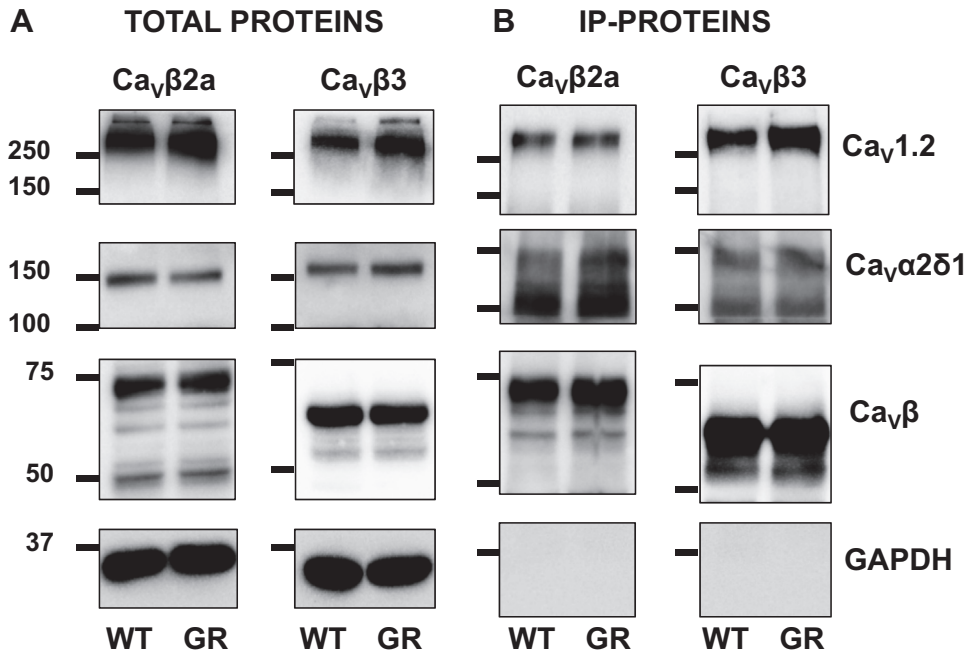

Figure 2. G449R interacts with $Ca_V\beta$ proteins. HEKT cells were transiently transfected with $Ca_V1.2$ WT (WT) or $Ca_V1.2$ G449R (GR) with cMyc-tagged $Ca_V\beta3$ or cMyc-tagged $Ca_V\beta2a$. $Ca_V\alpha2\delta1$ was present throughout. Cell lysates were immunoprecipitated overnight with anti-cMyc magnetic beads (Pierce Anti-c-Myc Magnetic Beads; catalog no.: 88842, Thermo Fisher Scientific) to capture the $Ca_V\beta$, eluted in a 2× Laemmli buffer and fractionated by 8% SDS-PAGE gels. *A*, immunoblotting was carried out on total proteins (20 μg) collected from the cell lysates before the immunoprecipitation assay (total proteins). The signal for the housekeeping protein GAPDH is shown below each blot. *B*, immunoblotting of "IP-proteins" was carried out after eluting the protein complexes from the beads. All immunoblots were carried out in parallel under the same transfection and extraction conditions. Western blotting was carried out with either anti-$Ca_V\beta3$ (Alomone; catalog no.: ACC008, 1:10,000 dilution), anti-$Ca_V\beta2a$ (Alomone; catalog no.: ACC105, 1:1000 dilution), anti-$Ca_V1.2$ directed against $Ca_V\alpha1C$ (Alomone; catalog no.: ACC003, 1:250 dilution), anti-$Ca_V\alpha2\delta1$ (Alomone; catalog no.: ACC015, 1:1000 dilution), and GAPDH (Sigma; 1:10,000 dilution) with an anti-rabbit as secondary antibody (Jackson ImmunoResearch; 1:10,000 dilution). Signals were detected with the enhanced chemiluminescence substrate. Blots were visualized with the ChemiDoc Touch system (Bio-Rad). Molecular weights were estimated using Image Lab software, version 5.2 (Bio-Rad) by linear regression of standard molecular weight markers. GAPDH, $Ca_V\beta3$, $Ca_V\beta2a$, $Ca_V\alpha2\delta1$, and $Ca_V1.2$ proteins migrated (in kilodalton) at 35, 60, 80, 175, and 250 kDa, respectively. From *left* to *right* in *A* and *B*: lane 1: $Ca_V1.2$ WT + $Ca_V\alpha2\delta1$ + $Ca_V\beta2a$; lane 2: $Ca_V1.2$ G449R + $Ca_V\alpha2\delta1$ + $Ca_V\beta2a$; lane 3: $Ca_V1.2$ WT + $Ca_V\alpha2\delta1$ + $Ca_V\beta3$; and lane 4: $Ca_V1.2$ G449R + $Ca_V\alpha2\delta1$ + $Ca_V\beta3$. HEKT, human embryonic kidney 293T cell line; IP, immunoprecipitation.

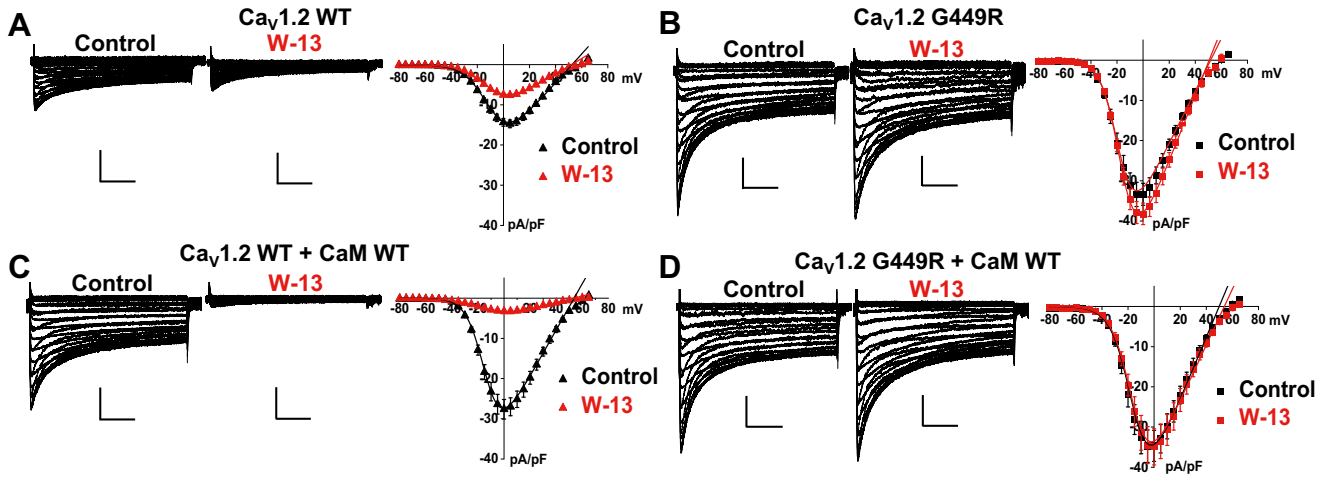

Figure 3. $Ca_V1.2$ G449R is insensitive to W-13. *A*, representative $Ca_V1.2$ WT current traces recorded in the presence of native/endogenous CaM from HEKT cells before (*left*) and after (*middle*) the application of W-13. Peak current densities of $Ca_V1.2$ WT currents are plotted against the applied voltages and fitted by a Boltzmann equation (*right*). Incubation with 10 μM W-13 for 15 min reduced the $Ca_V1.2$ WT current density by approximately 50%, from −15 ± 4 pA/pF under control conditions *versus* −8 ± 2 pA/pF in the presence of W-13. *B*, representative $Ca_V1.2$ G449R current traces recorded in the presence of native/endogenous CaM from HEKT cells before (*left*) and after (*middle*) W-13 treatment. In contrast to $Ca_V1.2$ WT, $Ca_V1.2$ G449R currents were unaffected by the W-13 and did not display any inhibition in the peak current density (*right*). *C*, representative $Ca_V1.2$ WT current traces cotransfected with CaM WT recorded from HEKT cells before (*left*) and after (*middle*) W-13 treatment. Overexpression of CaM WT significantly enhanced the current density of $Ca_V1.2$ WT, whereas only approximately, 10% of peak $Ca_V1.2$ currents remained following W-13 treatment (*right*). Peak current densities of $Ca_V1.2$ WT coexpressed with CaM WT are plotted against the applied voltages and fitted by a Boltzmann-like equation. *D*, representative $Ca_V1.2$ G449R current traces cotransfected with CaM WT recorded from HEKT cells before (*left*) and after (*middle*) application of W-13. Unlike the $Ca_V1.2$ WT channels, overexpression of CaM WT did not alter the $Ca_V1.2$ G449R currents. Furthermore, inhibition of the $Ca_V1.2$ G449R peak currents by W-13 was undetectable (*right*). The *vertical scale bars* are 10 pA/pF, and the *horizontal scale bars* are 100 ms throughout. All biophysical values are reported in Tables 1–3. CaM, calmodulin; HEKT, human embryonic kidney 293T cell line.

reduced the noninactivating component of $Ca_V1.2$ at the end of 100 ms depolarization (R100) from 0.65 ± 0.04 to 0.57 ± 0.02 ($p < 0.001$) (Table 1). Of note, W-13 did not impair Ca^{2+}-dependent facilitation in cardiac cells (40). Under the same experimental conditions, the inhibitory effect of W-13 on the current amplitude and the acceleration of current decay were blunted in the G449R construct with −33 ± 12 *versus* −38 ± 8 pA/pF (Fig. 3*B*) suggesting that the glycine substitution prevents the channel modulation by endogenous CaM.

CaM promotes the activity of $Ca_V1.2$ WT

In a typical cellular environment, CaM targets could far exceed that of free endogenous CaM (41, 42). To further explore the regulation by CaM, CaM WT was overexpressed along with the complementary DNA (cDNA) coding for the channel subunits. Overexpressing CaM has been shown to compete with endogenous CaM WT and was successfully used to reveal the mechanistic actions of CaM on voltage-activated Ca^{2+} channels (43–46). Representative current traces from cells coexpressing $Ca_V1.2$ WT and CaM WT are shown in Figure 3*C*. As seen, under these conditions, the peak current density nearly doubled up from −15 ± 4 to −28 ± 8 pA/pF ($p <$ 0.001 as compared with endogenous CaM) to reach values not significantly different than G449R under the same conditions ($p > 0.05$). CaM WT shifted the $E_{0.5,act}$ to hyperpolarized potentials ($p < 0.05$) and slightly accelerated the inactivation kinetics (Table 2). CaM enhanced the fraction of $Ca_V1.2$ WT currents that was inhibited by W-13, with about 90% reduction in peak current density, from 28 ± 8 pA/pF for control *versus* 3.3 ± 0.7 pA/pF for W-13 ($p = 0.001$). Overexpressing CaM WT caused undetectable changes in the peak current density, the voltage of activation, and the current decay of G449R that remained unaffected by the W-13 treatment (Fig. 3*D*) (Table 3). G449R functionally behaved like it intrinsically adopted a maximally active mode (47).

CaM was previously shown to bind to the I–II linker in addition to other intracellular sites within $Ca_V1.2$ (48). Pull-down assays demonstrated that CaM is tethered to the WT and the G449R channel complex (Fig. 4). In fact, the protein signal for G449R appeared to be more intense, hinting that it could maintain a stronger interaction with CaM. Enhanced channel activity could arise because of improved activation gating and/or increase in the relative cell surface protein expression/stability. Previous studies have reported that CaM enhances trafficking of $Ca_V1.2$ in human embryonic kidney (HEK) cells (49). CaM-induced increases in peak current density may reflect an improved surface expression of channel complexes. To sort this issue, we performed a series of cell fractionation assays. As seen in Figure 5 in the presence of endogenous CaM, the signal for $Ca_V1.2$ WT was stronger in the total membrane protein fraction (Fig. 5*A*, lane 3) than in the cell surface protein fraction (Fig. 5*A*, lane 4). Under the same conditions, the signal for $Ca_V1.2$ G449R was stronger in the cell surface protein fraction suggesting that G449R is better trafficked or more stable than channel complexes including the WT protein and endogenous CaM. Differences in the relative channel expression were obliterated when the channel complexes were overexpressed with CaM WT (Fig. 5*B*). Under these conditions, the WT and G449R channel complexes are similarly found in the cell surface fraction. Overexpression of CaM enhanced the cell surface trafficking of

Table 2
Electrophysiological properties of $Ca_V1.2$ WT with CaM WT and phosphorylation surrogates

			Electrophysiological properties		
$Ca_V1.2$	CaM	n/N	Peak current density (pA/pF)	$E_{0.5,act}$ (mV)	R100
$Ca_V1.2$ WT	CaM WT	28/6	−28 ± 8 $p < 0.001$ *versus* native CaM	−14 ± 3 $p = 0.002$ *versus* native CaM	0.60 ± 0.03 $p < 0.001$ *versus* native CaM
	+W-13	9/2	−3.3 ± 0.7 $p = 0.001$ *versus* control	−14 ± 3	0.65 ± 0.03 $p = 0.002$ *versus* control
	CaM T79A	18/2	−13 ± 5 $p < 0.001$ *versus* CaM WT, T79D, S81D	−13 ± 2	0.69 ± 0.03 $p < 0.01$ *versus* native CaM $p < 0.01$ *versus* CaM T79D, S81D
	+W-13	16/2	−14 ± 3	−14 ± 3	0.56 ± 0.03 $p < 0.001$ *versus* control
	CaM T79D	15/4	−29 ± 7 $p < 0.001$ *versus* native CaM $p < 0.001$ *versus* CaM T79A, S81A	−15 ± 3 $p < 0.001$ *versus* native CaM	0.55 ± 0.03 $p < 0.001$ *versus* native CaM $p < 0.001$ *versus* CaM WT, T79A, S81A, S81D
	+W-13	10/2	−4 ± 1 $p < 0.001$ *versus* control	−12 ± 2	0.71 ± 0.02 $p < 0.001$ *versus* control
	CaM S81A	17/2	−13 ± 4 $p < 0.001$ *versus* CaM WT, T79D, S81D	−13 ± 2	0.66 ± 0.03 $p < 0.01$ *versus* CaM WT, T79D, S81D
	+W-13	8/1	−12 ± 2	−9 ± 3	0.61 ± 0.02 $p = 0.02$ *versus* control
	CaM S81D	14/1	−32 ± 8 $p = 0.001$ *versus* native CaM $p = 0.001$ *versus* CaM T79A, S81A	−13 ± 3	0.62 ± 0.02 $p < 0.01$ *versus* CaM T79A, T79D, S81A
	+W-13	9/1	−5 ± 1 $p < 0.001$ *versus* control	−12 ± 2	0.70 ± 0.02 $p < 0.001$ *versus* control

Effects of CaM inhibitor W-13 on the biophysical properties of $Ca_V1.2$ WT channels. $Ca_V1.2$ WT was coexpressed with $Ca_V\beta2a$, $Ca_V\alpha2\delta1$, and CaM WT or phosphoresistant and phosphomimetic variants (T79A, T79D, S81A, or S81D). Activation properties ($E_{0.5,act}$) were estimated from the *I–V* relationships and fitted as described in the Experimental procedures section. The R100 values report the relative current decay observed 100 ms after the peak current. n/N refers to the number of cells/transfections measured in each condition of study. Mean ± SD are shown. Statistical significance of observed differences was evaluated using one-way ANOVA and Bonferroni test ($p < 0.05$). As seen, coexpression with CaM WT, CaM T79D, or T81D potentiated Ca^{2+} currents that were sensitive to CaM antagonists and sped up current decay. In contrast, coexpression with CaM T79A or CaM S81A (phosphoresistant analogs) produced Ca^{2+} currents similar to the ones measured in the presence of endogenous/native CaM in terms of peak current density and current decay. Nonetheless, CaM T79A and CaM S81A did not prevent the robust activation and rendered Ca^{2+} currents insensitive to inhibition by W-13.

$Ca_V1.2$ WT, which can account in part for the increased peak current density and possibly the increase in the activation gating.

Phosphomimetic surrogates of CaM are associated with increased activity of $Ca_V1.2$ WT

The precise mechanism though which W-13 inhibits CaM is not currently known, but it has been shown that W-13 bends the flexible linker of CaM between Met78 and Glu82 (50, 51), a region that harbors two important phosphorylation sites Thr79 and Ser81 (52). Phosphorylation at these two sites causes structural changes in the relative orientation of the C- and N-lobes, which in turn modulate the interaction of CaM with its protein targets (53, 54). To evaluate the structural properties of the flexible linker, we introduced phosphomimetic and phosphoresistant mutations on CaM by individually changing phosphorylation sites Thr79 and Ser81 to alanine (A) or aspartate (D), respectively, the latter mimicking the negative charge change induced by post-translational modification.

Overexpression of phosphoresistant CaM T79A (Fig. 6*A*, *left*) or CaM S81A (Fig. 6C, *left*) abrogated the upregulation of

Table 3
Electrophysiological properties of $Ca_V1.2$ G449R with CaM WT and phosphorylation surrogates

			Electrophysiological properties		
$Ca_v1.2$	CaM	n/N	Peak current density (pA/pF)	$E_{0.5,act}$ (mV)	R100
$Ca_V1.2$ G449R	CaM WT	20/3	−35 ± 10	−16 ± 2	0.50 ± 0.03
	+W-13	9/2	−35 ± 9	−17 ± 3	0.54 ± 0.01 $p = 0.04$ *versus* control
	CaM T79A	15/2	−32 ± 10	−16 ± 2	0.50 ± 0.02
	+W-13	14/2	−33 ± 10	−17 ± 3	0.45 ± 0.03 $p < 0.001$ *versus* control
	CaM T79D	24/3	−35 ± 9	−18 ± 4	0.50 ± 0.02
	+W-13	8/1	−32 ± 9	−16 ± 2	0.50 ± 0.02
	CaM S81A	13/1	−34 ± 9	−18 ± 2	0.48 ± 0.02 $p = 0.002$ *versus* native CaM $p = 0.02$ *versus* CaM S81D
	+W-13	9/1	−33 ± 7	−19 ± 2	0.51 ± 0.02
	CaM S81D	9/1	−35 ± 8	−17 ± 3	0.52 ± 0.02 $p = 0.02$ *versus* CaM S81A
	+W-13	10/1	−33 ± 10	−15 ± 3	0.50 ± 0.02

Effects of CaM inhibitor W-13 on the biophysical properties of $Ca_V1.2$ G449R channels. $Ca_V1.2$ G449R was coexpressed with $Ca_V\beta2a$, $Ca_V\alpha2\delta1$, and CaM WT or phosphoresistant and phosphomimetic variants (T79A, T79D, S81A, or S81D). Activation properties ($E_{0.5,act}$) were estimated from the *I–V* relationships and fitted as described in the Experimental procedures section. The R100 values report the relative current decay observed 100 ms after the peak current. n/N refers to the number of cells/transfections measured in each condition of study. Mean ± SD are shown. Statistical analysis was evaluated using one-way ANOVA and Bonferroni post hoc test. As seen, all experimental conditions yielded whole-cell Ca^{2+} currents that were not significantly different from one another ($p > 0.05$).

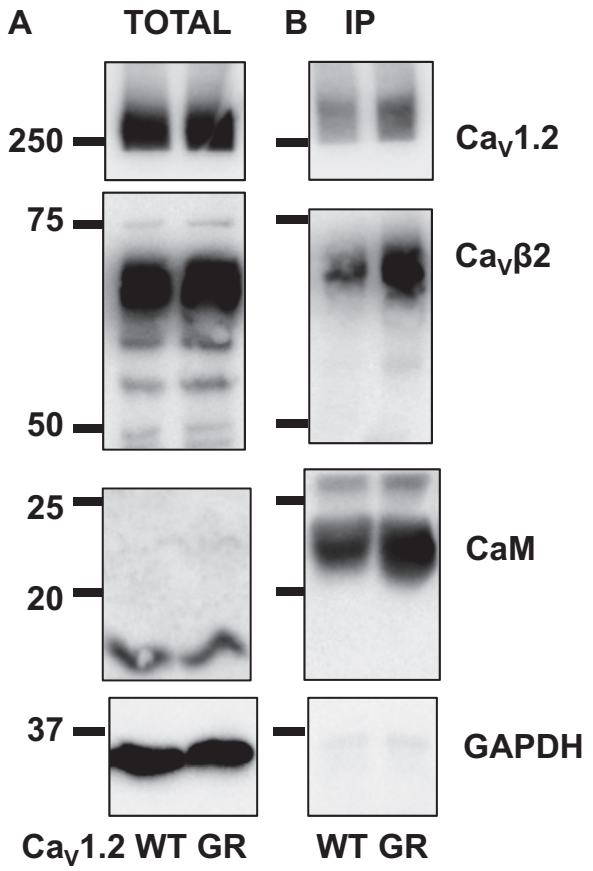

Figure 4. Calmodulin (CaM) pulls down the L-type calcium channel. HEKT cells were transiently transfected with $Ca_V\beta2a$, CaM WT, and either $Ca_V1.2$ WT (WT) or G449R (GR). CaM was captured by the anti-His–coated beads. *A*, proteins were homogenized, and a fraction of this solution (referred to as total) was set aside to validate protein expression. *B*, coimmunoprecipitation was carried out with anti-His magnetic beads. The bound proteins were eluted (referred to as pull-down) and electrophoresed on a 6% SDS-polyacrylamide gel or a 10% SDS-polyacrylamide gel for CaM and GAPDH before being transferred onto a nitrocellulose membrane. Western blotting was carried out with anti-$Ca_V\beta2$ (Alomone; catalog no.: ACC105, 1:1000 dilution), anti-$Ca_V1.2$ (Alomone; catalog no.: ACC003, 1:250 dilution) with an anti-rabbit as secondary antibody (Jackson ImmunoResearch, 1:10,000 dilution), and anti-CaM (Millipore; catalog no.: 05-193, 1:1000 dilution) with an anti-mouse as secondary antibody (Jackson ImmunoResearch, 1:10,000 dilution). Molecular weights were estimated using Image Lab software, version 5.2 (Bio-Rad) by linear regression of standard molecular weight markers. $Ca_V1.2$ WT and G449R, $Ca_V\beta2a$, and CaM proteins were translated at the expected molecular masses of 250, 70, and 18 to 24 kDa, respectively. $Ca_V1.2$ WT and G449R were successfully pulled indicating that $Ca_V1.2$ G449R interacts with $Ca_V\beta2a$ and CaM. This result was successfully obtained from four independent transfections carried out over the course of 3 months. HEKT, human embryonic kidney 293T cell line.

$Ca_V1.2$ WT currents by CaM WT. The peak current densities of $Ca_V1.2$ WT were −13 ± 5 pA/pF for CaM T79A ($p < 0.001$) and −13 ± 4 pA/pF for CaM S81A ($p < 0.001$) as compared with −28 ± 8 pA/pF when coexpressed with CaM WT (Table 2). The two phosphoresistant mutations failed to increase the peak current density and activation gating. Overexpression with phosphomimetic CaM variants T79D (Fig. 6*B*, *left*) or S81D (Fig. 6*D*, *left*) produced peak current densities and activation potentials comparable to those obtained with $Ca_V1.2$ WT + CaM WT (Fig. 6, *E* and *F*). The structural properties of the flexible linker were also shown to regulate the activity of Ca^{2+}-activated SK2 channels, although in this latter case, CaM T79D reduced channel activity (55).

CaM inhibitor W-13 substantially diminished $Ca_V1.2$ + CaM T79D or $Ca_V1.2$ + CaM S81D currents by around 85% (Fig. 6, *B* and *D*, *middle*) with values of −4 ± 1 pA/pF (Fig. 6*B*, *right*) and −5 ± 1 pA/pF, respectively (Fig. 6*D*, *right*). Treatment with W-13 did not however further inhibit $Ca_V1.2$ channels coexpressed with phosphoresistant CaM T79A and S81A (Fig. 6*A* and *C*, *middle* and *right*; Fig. 6*E*) and had little impact on the activation gating under any of these conditions (Fig. 6*F* and Table 2).

The modulation of CaM WT on the function of $Ca_V1.2$ WT was equivalent to the action of phosphomimetic surrogates CaM T79D and S81D, suggesting that the phosphorylated form of CaM is responsible for the functional upregulation of $Ca_V1.2$. Roughly 10 to 45% of endogenous CaM is constitutively phosphorylated *in vivo* by casein kinase II (CK2) (52, 56, 57), and *in vitro* studies confirmed that CaM Thr79 and Ser81 are the most likely targets (58, 59). Experiments were thus performed in the presence of 4,5,6,7-tetrabromobenzotriazole (TBB; Tocris, Bio-Techne), a specific inhibitor of CK2. As shown in Table 4, TBB significantly decreased the peak current density by ≈70% and right shifted the activation gating of whole-cell currents recorded in the presence of $Ca_V1.2$ WT with native CaM. Furthermore, TBB annihilated the impact of overexpressing CaM WT on the peak current density of $Ca_V1.2$ WT. The impact of TBB was comparable to the disrupting effect of W-13 and much greater than the coexpression with either CaM T79A or S81A.

Ca^{2+} binding to CaM remains a prerequisite step for driving the channel complex into its higher functioning mode. Overexpression of the Ca^{2+}-free form of CaM (CaM1234 or CaM D20A/D56A/D93A/D129A) decelerated, as expected, the CDI kinetics (Table 5). It also abrogated the increased peak current density and restored its activation gating to the level observed in the presence of endogenous CaM.

The gain of function in $Ca_V1.2$ G449R requires the Ca^{2+}-bound CaM form

Unlike $Ca_V1.2$ WT, coexpressing either phosphoresistant CaM T79A (Fig. 7*A*, *left*) and S81A (Fig. 7*C*, *left*) or phosphomimetic CaM T79D (Fig. 7*B*, *left*) and S81D (Fig. 7*D*, *left*) with Cav1.2 G449R did not appreciably affect the peak current density, activation gating kinetics ($E_{0.5,act}$), and current decay (R100) of $Ca_V1.2$ G449R (Fig. 7, *E* and *F* and Table 3). As observed in the presence of CaM WT, the peak current densities (Fig. 7, *A*–*D*, *middle*, *right*; Fig. 7*E*), the $E_{0.5,act}$ (Fig. 7*F*) were not altered by the application of W-13. This sharply contrasts with the results obtained with the $Ca_V1.2$ WT channel complex. Nonetheless, preventing the phosphorylation of all CaM molecules with TBB reduced by 50% the peak current density measured under all other conditions (Table 4) save for CaM1234 (Table 5). Indeed, limiting Ca^{2+} binding to CaM with the CaM1234 variant not only impaired the CDI of $Ca_V1.2$ G449R but also prevented the leftward shift in activation gating and the increase in peak current density (Table 5).

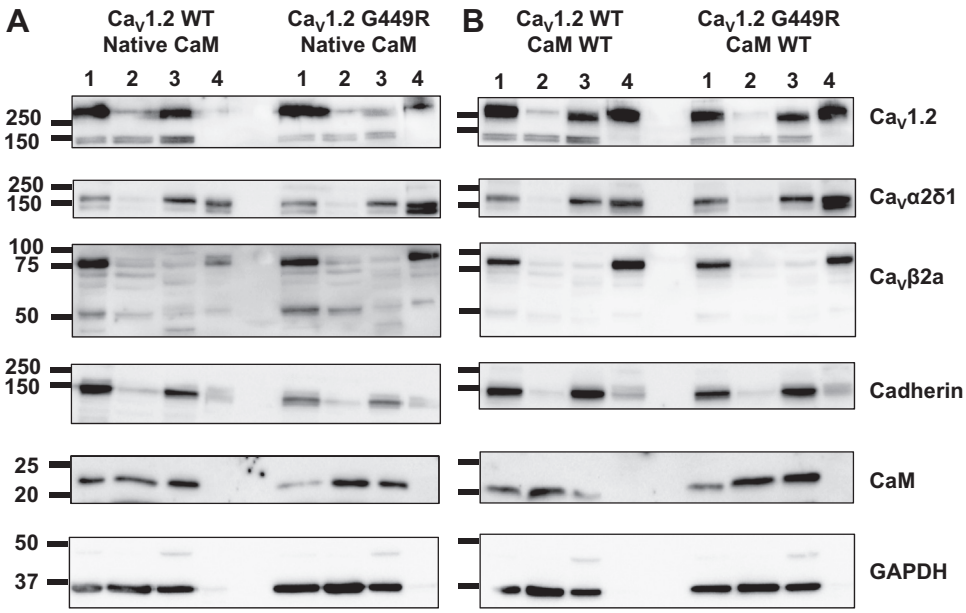

Figure 5. CaM promotes the cell surface localization of Ca$_V$1.2 WT but not Ca$_V$1.2 G449R. *A*, HEKT cells were transiently transfected with Ca$_V$1.2 WT + Ca$_V$α2δ1 + Ca$_V$β2a (*left*) and Ca$_V$1.2 G449R + Ca$_V$α2δ1 + Ca$_V$β2a (*right*) in the presence of native/endogenous CaM. *B*, HEKT cells were transiently transfected with Ca$_V$1.2 WT + Ca$_V$α2δ1 + Ca$_V$β2a + CaM WT (*left*) and Ca$_V$1.2 G449R + Ca$_V$α2δ1 + Ca$_V$β2a + CaM WT (*right*). Two days after transfection, the cells were lysed, and cell fractions were obtained through preparative ultracentrifugation as described in the Experimental procedures section. Western blotting was carried out for the four protein fractions found in lanes 1 to 4; lane 1: total proteins; lane 2: cytoplasmic proteins; lane 3: total membrane proteins; and lane 4: plasma membrane proteins. The proteins were probed with the following antibodies: Ca$_V$1.2 (Alomone; catalog no.: ACC003, 1:250 dilution) with anti-rabbit (1:10,000 dilution); Ca$_V$α2δ1 (Alomone; catalog no.: ACC015, 1:1000 dilution) with anti-rabbit (1:10,000 dilution); Ca$_V$β2a (Alomone; catalog no.: ACC105, 1:1000 dilution) with anti-rabbit (1:10,000 dilution); CaM (Millipore; catalog no.: 05-193, 1:1000 dilution) with anti-mouse (1:10,000 dilution); His (Invitrogen; catalog no.: 71700, 1:1000 dilution) with anti-mouse (1:10,000 dilution); and cadherin (Pan-cadherin; Thermo Fisher; catalog no.: 71-7100, 1:1000 dilution) with anti-rabbit (1:10,000). Cadherin was used as a marker for the plasma membrane. The membrane was cut at 115 and 28 kDa to probe first Ca$_V$1.2, Ca$_V$β2a, and CaM. Membranes were then stripped and reprobed with antibodies against the proteins: Ca$_V$α2δ1, cadherin, and housekeeping GAPDH (Sigma; catalog no.: G9545, 1:10,000 dilution with anti-rabbit [1:10,000 dilution]). Each lane was loaded with 20 μg proteins. The *lines* to the *left* of the blots indicate the position of the molecular markers, and the value is provided in kilodalton. The molecular masses were estimated by linear regression and interpolation from the molecular mass markers using the Image Lab software, version 5.2 (Bio-Rad). As seen in *A*, in the presence of endogenous CaM, the signal for Ca$_V$1.2 WT was stronger in the total membrane protein fraction (lane 3) than in the cell surface protein fraction (lane 4). Under the same conditions, the signal for Ca$_V$1.2 G449R was stronger in the cell surface protein fraction. *B*, demonstrates that under conditions where CaM was overexpressed, the signal for Ca$_V$1.2 WT and Ca$_V$1.2 G449R is stronger in the cell surface protein fraction. Along with Ca$_V$1.2, Ca$_V$α2δ1 (as previously reported (4)) and Ca$_V$β2a are found in the cell surface fraction but not CaM and GAPDH. This observation suggests that the interaction of CaM with the pore-forming subunit is very robust during the cell surface export and is compatible with the binding and unbinding kinetics of CaM in other cell types (42). No significant signal was found in the cytoplasmic fraction for Ca$_V$α2δ1 and the membrane-anchored Ca$_V$β2a. This result was successfully obtained from two independent transfections carried out over the course of 2 months. CaM, calmodulin; HEKT, human embryonic kidney 293T cell line.

Alanine substitutions in the hinge region of CaM are not disrupting interaction with Ca$_V$1.2

We next evaluated whether CaM variants T79A and S81A alter the interaction of CaM with the pore-forming Ca$_V$α1C subunit (Fig. 8). Whether for Ca$_V$1.2 WT or Ca$_V$1.2 G449R, the pull-down assays failed to reveal a correlation between the signal intensity and any of the tested CaM-substituted proteins indicating that phosphomimetic analogs of Ca^{2+}-bound CaM impact channel function rather than protein interaction. Nonetheless, coimmunoprecipitation assays performed over a 1-year period consistently revealed a stronger signal for G449R proteins than for Ca$_V$1.2 WT proteins suggesting that the glycine to arginine substitution at position 449 could increase the affinity of CaM for Ca$_V$1.2.

Substitution with an alpha-helix breaker in Ca$_V$1.2 antagonizes channel function

The structural properties of the I–II linker near the high-affinity binding site for Ca$_V$β have been consistently shown to modulate the gating properties of Ca$_V$1 and Ca$_V$2 channels (31). In Ca$_V$1.2, most, if not all substitutions, tested at position 449 altered the channel properties. Stronger activation gating and faster inactivation kinetics characterized Ca$_V$1.2 G449A, G449D, and G449K in the presence of endogenous CaM (Fig. S1 and Table 6). All these substituted channels activated at more hyperpolarized voltages than Ca$_V$1.2 WT with a threshold at −40 mV and currents peaking between 0 and −5 mV. These data could suggest that α-helix-enhancing residues and/or positively charged residues increase the channel affinity for CaM. Hence, the CaM–channel complex would be very stable in the presence of endogenous CaM as to avert the impact of CaM mutants. To test the role of the secondary structure, position 449 in Ca$_V$1.2 was substituted with proline, recognized as α-helix breaker (60). G449P produced whole-cell peak currents (−2.5 ± 0.8 pA/pF, n = 10, N = 2, $p < 0.001$ *versus* Ca$_V$1.2 WT) that were five times smaller than Ca$_V$1.2 WT but significantly different than voltage-activated inward Ca^{2+} currents measured in nontransfected cells. The activation gating of G449P was right shifted when compared with Ca$_V$1.2 WT. In contrast to G449R and G449K, Ca$_V$1.2 G449P was modulated by CaM phosphomimetic

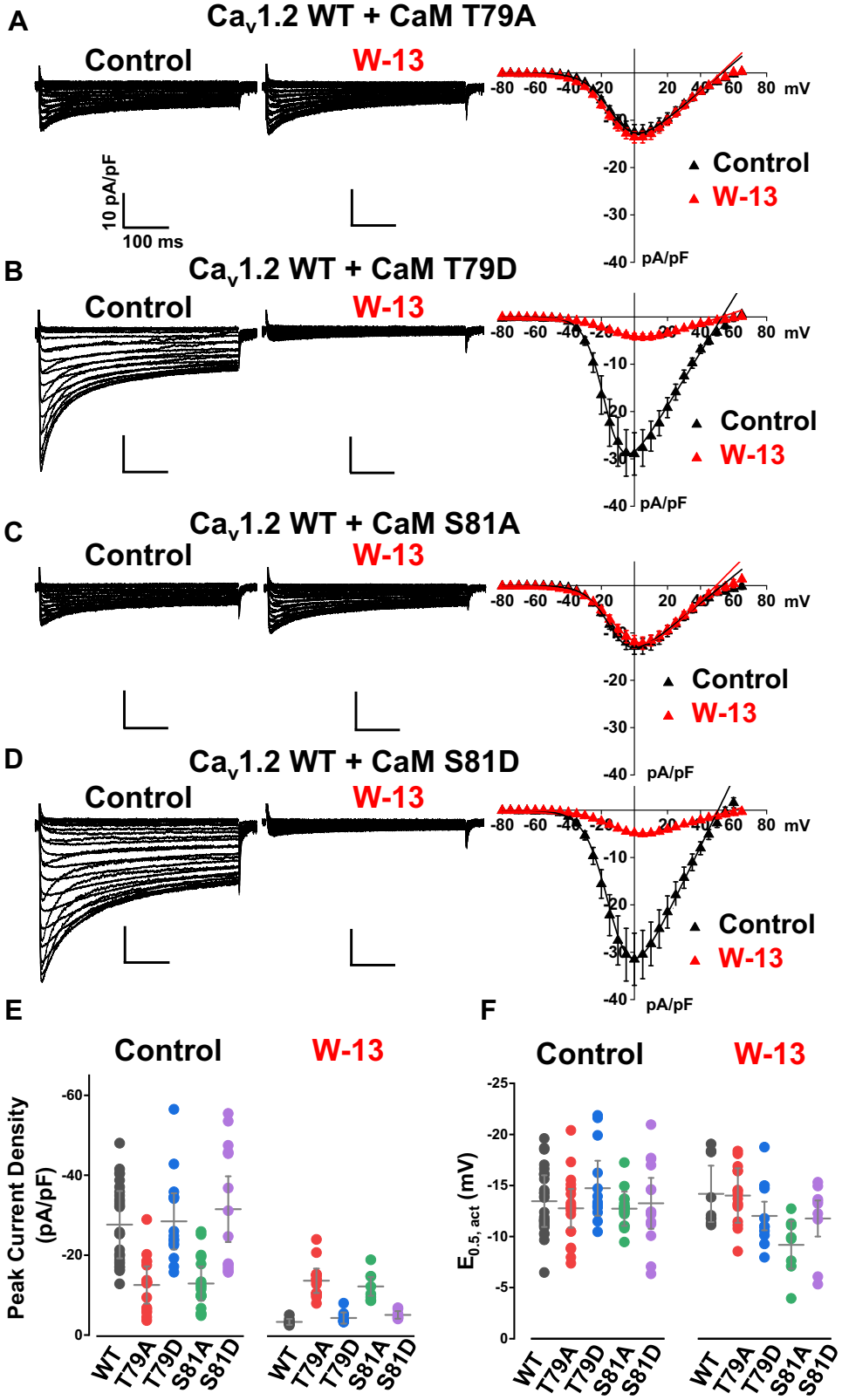

Figure 6. Phosphomimetic CaM T79D and S81D upregulate Ca$_v$1.2 WT channels. *A* and *C*, *middle*, Ca$_v$1.2 WT was coexpressed with the "phosphor-esistant" CaM mutations T79A or S81A. Overexpression of CaM T79A or S81A failed to enhance the currents and was insensitive to W-13. *A* and *C*, *right*, average *I–V* curves of Ca$_v$1.2 WT coexpressed with CaM T79A or S81A. The peak current densities were not different between control and W-13 treatment. *B* and *D*, *left*, *middle*, Ca$_v$1.2 WT current traces recorded from HEKT cells after coexpression with phosphomimetic CaM T79D or S81D. Overexpression of CaM T79D or CaM S81D boosted Ca$_v$1.2 peak currents that were sharply abolished by the extracellular application of W-13. The *vertical scale bars* are 10 pA/pF, and the *horizontal scale bars* are 100 ms throughout. *B* and *D*, *right*, average *I–V* curves of Ca$_v$1.2 WT coexpressed with CaM T79D or S81D for control and W-13 treatment. *E* and *F*, the distribution of the peak current densities and $E_{0.5,act}$ for control and W-13 are summarized as *filled circles* for Ca$_v$1.2 WT coexpressed with either CaM WT (*black*), T79A (*red*), T79D (*blue*), S81A (*green*), or S81D (*light purple*). The mean data ± SD are shown as *gray hyphens*. The values of the average peak current densities and $E_{0.5,act}$ are listed in Table 2. CaM, calmodulin; HEKT, human embryonic kidney 293T cell line.

Table 4
Electrophysiological properties of $Ca_V1.2$ WT and G449R with TBB

			Electrophysiological properties		
$Ca_V1.2$	CaM	n/N	Peak current density (pA/pF)	$E_{0.5,act}$ (mV)	R100
$Ca_V1.2$ WT	Native CaM	30/7	−15 ± 4	−10 ± 3	0.65 ± 0.04
	+TBB	6/2	−4 ± 1	−5 ± 1	0.80 ± 0.01
			p = 0.001 *versus* control	p = 0.001 *versus* control	p < 0.001 *versus* control
	CaM WT	28/6	−28 ± 8	−14 ± 3	0.60 ± 0.03
	+TBB	5/1	−4.9 ± 0.7	−8 ± 2	0.73 ± 0.01
			p < 0.001 *versus* control	p = 0.001 *versus* control	p < 0.001 *versus* control
$Ca_V1.2$ G449R	Native CaM	31/4	−33 ± 12	−17 ± 3	0.52 ± 0.03
	+TBB	7/2	−15 ± 6	−15 ± 3	0.55 ± 0.03
			p = 0.001 *versus* control		
	CaM WT	20/3	−35 ± 10	−16 ± 2	0.50 ± 0.03
	+TBB	7/2	−13 ± 5	−13 ± 4	0.57 ± 0.03
			p < 0.001 *versus* control	p = 0.06 *versus* control	p < 0.01 *versus* control

Effects of TBB, the cell-permeable inhibitor of CK2 on the biophysical properties of $Ca_V1.2$ WT and $Ca_V1.2$ G449R channels. $Ca_V1.2$ (WT or G449R) was coexpressed with $Ca_V\beta2a$, $Ca_V\alpha2\delta1$, and CaM WT as indicated. Two days after transfection, experiments were performed in the presence of 2.5 μM TBB, usually regarded as a membrane-permeable specific inhibitor of CK2. Activation properties ($E_{0.5,act}$) were estimated from the *I–V* relationships and fitted as described in the Experimental procedures section. The R100 values report the relative current decay observed 100 ms after the peak current. n/N refers to the number of cells/transfections measured in each condition of the study. Mean ± SD are shown. Statistical analysis was evaluated using one-way ANOVA and Bonferroni post hoc test. As seen, TBB significantly decreased the channel peak current density under all conditions. It also significantly right shifted the activation gating of $Ca_V1.2$ WT but not of $Ca_V1.2$ G449R.

variants (Fig. 9 and Table 6). Peak currents of G449P nearly tripled in the presence of CaM WT, CaM T79D, or CaM S81D and were not significantly altered by coexpressing CaM T79A or CaM S81A (Fig. 9, *A* and *B*). Remarkably, the activation of the G449P channel was left shifted in the presence of the phosphor-silenced CaM variants (Fig. 9*D*), the only occurrence where the larger peak currents were not associated with stronger activation gating. Altogether, these observations support a strong mechanistic link between the structural properties of the I–II linker near the binding site for $Ca_V\beta$ and the modulation of the channel activation gating by CaM. In particular, the channel propensity to adopt a longer α-helix in this region appears to improve the activation gating of the channel and to supersede the modulation by the phosphorylated forms of CaM.

Discussion

Ca^{2+}–CaM modulates the activity of L-type $Ca_V1.2$ through multifaceted mechanisms

The ubiquitous multifunctional Ca^{2+}-binding protein CaM is a two-lobe protein with each of two hydrophilic pockets for Ca^{2+} sensing separated by a flexible central linker. It is regulating the function of many voltage-gated ion channels, such as Kv7.2 (61), $Na_V1.4$ (7), and in particular, voltage-gated Ca_V channels (7, 62) (for review, see Ref. (62)). At least two CaM molecules can simultaneously bind to the C-terminal region of $Ca_V1.2$ (63, 64), but additional binding sites in the N-terminal region and the first intracellular linker of $Ca_V\alpha1C$ have been identified (48, 63, 65–67). The overall structural organization of CaM within the $Ca_V1.2$ channel complex remains to be established. CaM-binding sites were not resolved in the cryo-electron microscopy structure of the homologous $Ca_V1.1$ channel (3).

In $Ca_V1.2$ channels, Ca^{2+} binding to CaM contributes to CDI and Ca^{2+}-dependent facilitation (7–9). Either process requires the binding of incoming Ca^{2+} ions to CaM pre-associated to the isoleucine–glutamine motif in the C-terminal region of the pore-forming $Ca_V\alpha1C$ subunit (10–13). The potentiating form of CaM-dependent facilitation or upregulation is observed in native cardiac L-type channels during trains of depolarization (68, 69) but usually not reported in recombinant systems with the intact $Ca_V1.2$ WT channel (8, 9, 29). We herein report that phosphomimetic analogs of CaM stimulate Ca^{2+} influx and promotes the activation gating of $Ca_V1.2$. CaM promotes the cell surface trafficking of $Ca_V1.2$ and stimulates function through an increase in peak current density and a leftward shift in the activation gating. In our

Table 5
Effect of CaM1234 on electrophysiological properties of $Ca_V1.2$ WT and $Ca_V1.2$ G449R

			Electrophysiological properties		
$Ca_V1.2$	CaM	n/N	Peak current density (pA/pF)	$E_{0.5,act}$ (mV)	R100
$Ca_V1.2$ WT	CaM1234	10/2	−9 ± 2	−6 ± 2	0.76 ± 0.02
			p < 0.001 *versus* CaM WT	p < 0.001 *versus* CaM WT	p < 0.001 *versus* CaM WT
	+W-13	7/1	−4 ± 2	−5 ± 2	0.71 ± 0.02
			p =0.04 *versus* control		p < 0.001 *versus* control
$Ca_V1.2$ G449R	CaM1234	4/2	−17 ± 4	−10 ± 2	0.73 ± 0.01
			p < 0.001 *versus* CaM WT	p < 0.001 *versus* CaM WT	p < 0.001 *versus* CaM WT
	+W-13	6/1	−19 ± 2	−10 ± 2	0.63 ± 0.01
					p < 0.001 *versus* control

Whole-cell currents were recorded from HEKT cells transiently transfected with $Ca_V1.2$ WT or variants coexpressed with $Ca_V\beta2a$, $Ca_V\alpha2\delta1$, and CaM1234. Activation properties ($E_{0.5,act}$) were estimated from the *I–V* relationships and fitted to a BoltzIV equation as described in the Experimental procedures section. The R100 values report the relative current decay observed 100 ms after the peak current. n/N refers to the number of cells/transfections measured in each condition of study. Mean ± SD are shown. Statistical analysis was carried out against the values measured for CaM WT. Herein "control" refers to the data collected in the presence of CaM1234 in the absence of W-13.

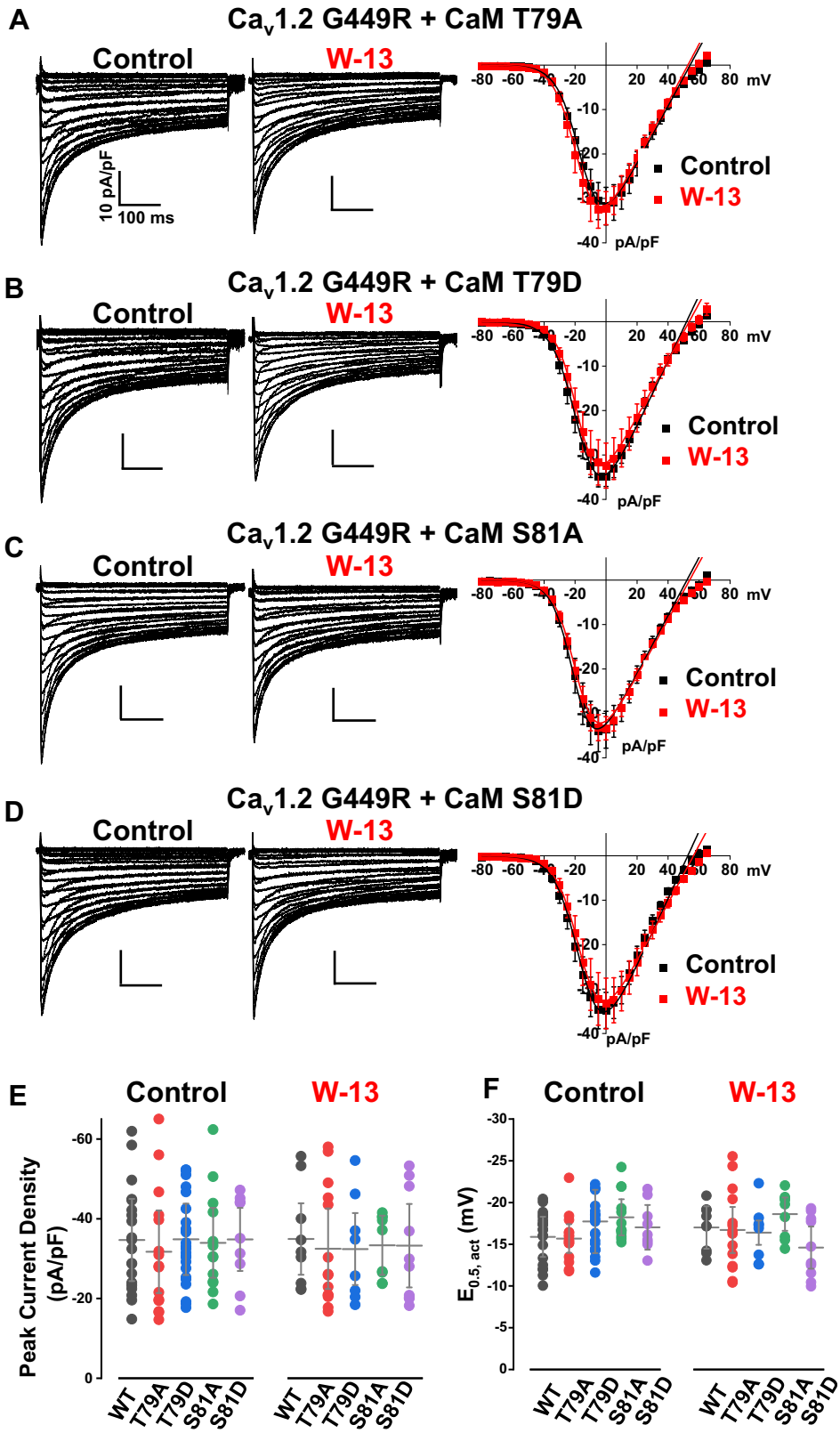

Figure 7. CaV1.2 G449R is not modulated by CaM or CaM inhibitor W-13. Representative $Ca_V1.2$ G449R current traces were recorded from HEKT cells in the presence of 2 mM Ca^{2+}. *A–D*, *left*, $Ca_V1.2$ G449R was coexpressed with CaM WT, with the phosphoresistant CaM (T79A or S81A) or with phosphomimetic CaM (T79D or S81D) as shown. *A–D*, *middle*, $Ca_V1.2$ G449R channels coexpressed with either CaM WT, T79A, T79D, S81A, or S81D are resistant to block by W-13. The *vertical scale bars* are 10 pA/pF, and the *horizontal scale bars* are 100 ms throughout. *A–D*, *right*, average *I–V* curves of $Ca_V1.2$ G449R coexpressed with CaM T79A, T79D, S81A, or S81D. The peak current densities were not different between control and W-13 treatment. *E* and *F*, the distribution of the peak current densities and $E_{0.5,act}$ for control conditions and after W-13 treatment are summarized individually as *filled circles* for $Ca_V1.2$ G449R coexpressed with either CaM WT (*black*), T79A (*red*), T79D (*blue*), S81A (*green*), or S81D (*light purple*). The mean data ± SD are shown as *gray hyphens*. The complete set of values is found in Table 3. CaM, calmodulin; HEKT, human embryonic kidney 293T cell line.

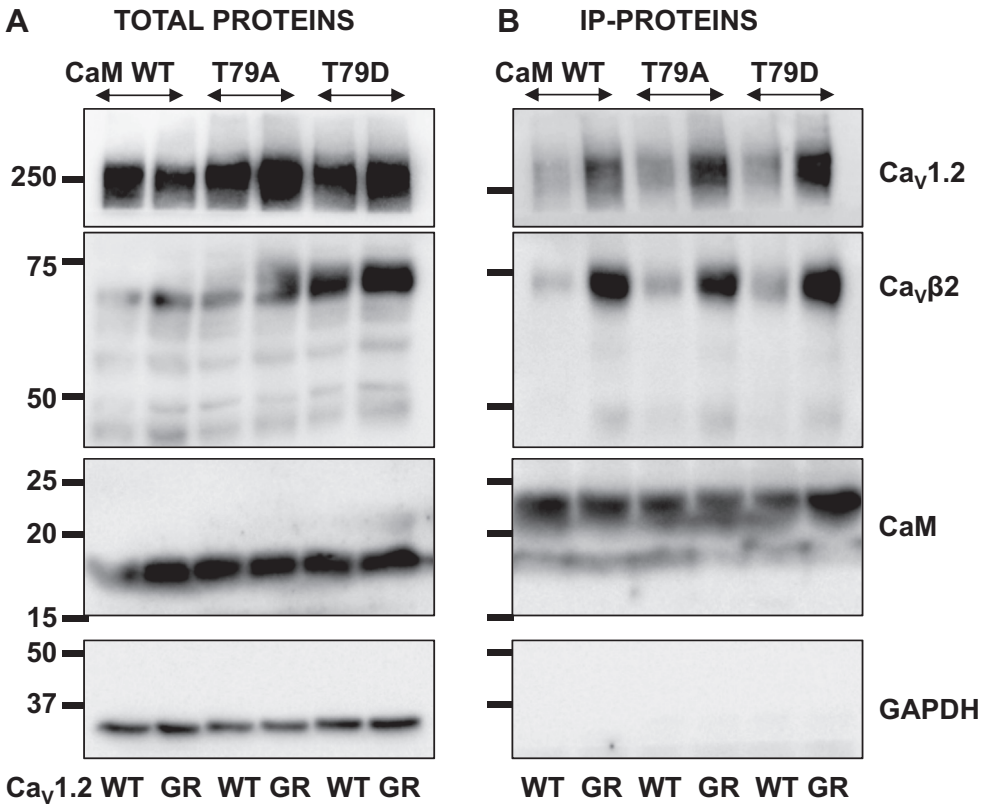

Figure 8. CaM T79A and T79D coimmunoprecipitate $Ca_V1.2$ WT and G449R. HEKT cells were transiently transfected with $Ca_V\beta2a$ in the presence of $Ca_V1.2$ WT or $Ca_V1.2$ G449R and either CaM WT, CaM T79A, or CaM T79D. *A*, total proteins are shown. *B*, coimmunoprecipitation was carried out with anti-His magnetic beads. Immunoblotting was carried out after elution of the bound proteins using the antibodies described in the legend of Figure 4. As seen, $Ca_V1.2$ WT and G449R, $Ca_V\beta2a$, and CaM proteins were translated at the expected molecular masses of 250, 70, and 18 to 24 kDa, respectively. There was no significant difference between the signals measured in the presence of either CaM WT, CaM T79A, or CaM T79D. The signals were nonetheless systematically stronger for $Ca_V1.2$ G449R than for $Ca_V1.2$ WT despite equivalent loading and similar signals for the total proteins. Similar data were obtained from three independent transfections carried out over the course of 2 months with protein extraction carried out with digitonin or CHAPS. CaM, calmodulin; HEKT, human embryonic kidney 293T cell line.

hands, the latter actions of CaM require Ca^{2+} as it was impaired in the presence of the constitutively Ca^{2+}-free form CaM1234 where the four Ca^{2+}-binding sites are invalidated. This observation is compatible with data from Kim *et al.* (70), who reported that the interaction between the CaM-bound C-terminal peptide and the I–II linker is disrupted in the complete absence of Ca^{2+}. CaM1234 prevented the increase in peak current density, failed to promote channel activation gating, and as expected, slowed down the CDI kinetics by 30%. Nonetheless, Ca^{2+} binding is not sufficient to account for the wide-ranging impact of CaM on channel function. The structural properties of the flexible linker region of CaM contribute to the channel response to CaM. Coexpression with CaM T79A or CaM S81A averted the boost in peak current density (although it did not alter the activation gating). In contrast, coexpression with either CaM WT or phosphomimetic CaM T79D or CaM S81A yielded similar results suggesting that phosphorylation of either site participates to the modulation of $Ca_V1.2$ by CaM. Indeed, preventing the phosphorylation of native and overexpressed CaM by incubating the cells with TBB, a membrane-permeable inhibitor of CK2, nearly abrogated channel function. Hence, Ca^{2+}-bound CaM modulates the function of the $Ca_V1.2$ channel complex in a fashion reminiscent of the ancillary subunits $Ca_V\beta$ and $Ca_V\alpha2\delta$, which like CaM may also modulate other ion channels (71).

Multiple mechanisms converge toward $Ca_V1.2$ G449R

The missense variant, glycine to arginine, was identified from a patient with prolonged QT interval (≈500 ms) and features associated with the TS, but its heterologous expression revealed a novel phenotype where the gain of function resulted from increased peak current density, a negative shift in the activation potential, and no decrease in the channel current decay (28). The hyperactive mode of the variant expressed in HEK293T (thereafter referred to as HEKT) cells was mimicked by the coexpression of $Ca_V1.2$ WT with CaM WT or phosphorylated surrogates CaM T79D or CaM S81D. The functional properties of the clinical glycine to arginine variant remained remarkably insensitive to pharmacological inhibition by W-13 and by overexpression with phosphoresistant CaM analogs (T79A and S81A). The impact of the phosphorylation of CaM appears to be limited to function. $Ca_V1.2$ G449R was pulled down equally by CaM WT, T79A, and T79D. Preventing the phosphorylation of CaM with TBB, an inhibitor of CK2, significantly reduced the peak current density of $Ca_V1.2$ G449R by ≈50% without a significant

Table 6
Electrophysiological properties of $Ca_V1.2$ Gly449 variants with CaM phosphorylation surrogates

			Electrophysiological properties		
$Ca_V1.2$	CaM	n/N	Peak current density (pA/pF)	$E_{0.5,act}$ (mV)	R100
$Ca_V1.2$ G449A	Native	12/2	−35 ± 8	−18 ± 3	0.55 ± 0.03
	CaM WT	22/4	−31 ± 8	−15 ± 2	0.57 ± 0.03
	CaM T79A	7/1	−11 ± 2 $p < 0.001$ *versus* native CaM $p < 0.001$ *versus* CaM WT	−13 ± 2 $p = 0.002$ *versus* native CaM	0.70 ± 0.01 $p < 0.001$ *versus* native CaM $p < 0.001$ *versus* CaM WT
	CaM T79D	6/1	−28 ± 8	−18 ± 2	0.55 ± 0.02
	CaM S81A	13/2	−14 ± 3 $p < 0.001$ *versus* native CaM $p < 0.001$ *versus* CaM WT	−13 ± 2 $p < 0.001$ *versus* native CaM	0.70 ± 0.03 $p < 0.001$ *versus* native CaM $p < 0.001$ *versus* CaM WT
	CaM S81D	19/2	−30 ± 9	−14 ± 3 $p = 0.007$ *versus* native CaM	0.58 ± 0.03
$Ca_V1.2$ G449D	Native	17/2	−14 ± 4	−15 ± 2	0.62 ± 0.03
	CaM WT	17/2	−27 ± 8 $p < 0.001$ *versus* native CaM	−17 ± 2	0.56 ± 0.02 $p < 0.001$ *versus* native CaM
	CaM T79A	16/1	−15 ± 4 $p < 0.001$ *versus* CaM WT	−16 ± 3	0.59 ± 0.02 $p = 0.04$ *versus* native CaM $p = 0.002$ *versus* CaM WT
	CaM T79D	14/1	−29 ± 6 $p < 0.001$ *versus* native CaM	−18 ± 2 $p = 0.007$ *versus* native CaM	0.55 ± 0.02 $p < 0.001$ *versus* native CaM
	CaM S81A	21/2	−16 ± 4 $p < 0.001$ *versus* CaM WT	−15 ± 2	0.60 ± 0.02 $p < 0.001$ *versus* CaM WT
	CaM S81D	10/1	−33 ± 7 $p < 0.001$ *versus* native CaM	−18 ± 2 $p = 0.03$ *versus* native CaM	0.52 ± 0.02 $p < 0.001$ *versus* native CaM $p = 0.01$ *versus* CaM WT
$Ca_V1.2$ G449P	Native	10/2	−2.5 ± 0.8	−4 ± 1	0.72 ± 0.02
	CaM WT	8/2	−6 ± 1 $p < 0.001$ *versus* native CaM	1.0 ± 2 $p < 0.001$ *versus* native CaM	0.65 ± 0.02 $p < 0.001$ *versus* native CaM
	CaM T79A	3/1	−1.6 ± 0.3 $p = 0.001$ *versus* CaM WT	−9 ±1 $p = 0.04$ *versus* native CaM $p = 0.002$ *versus* CaM WT	0.76 ± 0.01 $p < 0.001$ *versus* CaM WT
	CaM T79D	4/1	−11 ± 3 $p < 0.001$ *versus* native CaM, CaM WT	−0.5 ± 1.5 p =0.01 *versus* native CaM	0.57 ± 0.01 $p < 0.001$ *versus* native CaM $p < 0.001$ *versus* CaM WT
	CaM S81A	4/1	−1.8 ± 0.5 $p < 0.001$ *versus* CaM WT	−10 ± 2 $p < 0.001$ *versus* native CaM $p < 0.001$ *versus* CaM WT	0.73 ± 0.02 $p < 0.001$ *versus* CaM WT
	CaM S81D	3/1	−9.7 ± 0.7 $p < 0.001$ *versus* native CaM $p = 0.01$ *versus* CaM WT	3.5 ± 0.7 $p < 0.001$ *versus* native CaM $p = 0.01$ *versus* CaM WT	0.69 ± 0.03
$Ca_V1.2$ G449K	Native	18/2	−23 ± 5	−15 ± 3	0.60 ± 0.02
	CaM WT	26/6	−26 ± 6	−15 ± 3	0.61 ± 0.03
	CaM T79A	8/1	−28 ± 7	−17 ± 2	0.57 ± 0.02 $p = 0.006$ *versus* CaM WT
	CaM T79D	12/1	−30 ± 6 $p = 0.02$ *versus* native CaM $p = 0.002$ *versus* CaM WT	−17 ± 2	0.54 ± 0.02 $p < 0.001$ *versus* native CaM $p < 0.001$ *versus* CaM WT
	CaM S81A	15/2	−27 ± 7	−16 ± 3	0.56 ± 0.03 $p < 0.001$ *versus* native CaM $p < 0.001$ *versus* CaM WT
	CaM S81D	15/2	−29 ± 5 $p = 0.01$ *versus* CaM WT	−17 ± 3	0.56 ± 0.03 $p < 0.001$ *versus* native CaM $p < 0.001$ *versus* CaM WT

$Ca_V1.2$ Gly449 variants were coexpressed with $Ca_V\beta2a$, $Ca_V\alpha2\delta1$, and CaM WT or CaM T79A, CaM T79D, CaM S81A, or CaM S81D. Activation properties ($E_{0.5,act}$) were estimated from the *I–V* relationships as described in the Experimental procedures section. n/N refers to the number of cells/transfections measured in each condition of study. Mean ± SD are shown. Statistical analysis was carried out against CaM WT or against endogenous/native CaM. As seen, $Ca_V1.2$ WT, G449D, and G449P were modulated by CaM phosphovariants, whereas the properties of G449K remained unaffected. G449A was not upregulated by CaM WT but was downregulated by phosphoresistant CaM variants.

alteration in the channel activation voltage as compared with the control conditions. The rate-limiting factor appears to be Ca^{2+} binding to CaM. Coexpression of G449R with the CaM1234 variant not only impaired the CDI and the increased peak current density but also prevented the leftward shift in activation gating. Overexpression of the CaM1234 variant obliterated the gain in the function of $Ca_V1.2$ G449R yielding an activity profile akin to $Ca_V1.2$ WT in the presence of endogenous/native CaM. The stronger activity of $Ca_V1.2$ G449 thus minimally requires the direct or indirect action of the Ca^{2+}-bound CaM form.

These observations suggest that the higher channel activity of G449R could result from a stronger affinity for native CaM. Though not measured in this article, the affinity between the two full-length proteins can be roughly approximated by the relative intensity of the signal measured in coimmunoprecipitation assays. Within all the limitations of this exercise, the protein signal obtained for G449R in coimmunoprecipitation assays was indeed systematically stronger than the signal measured for the WT channel complex when measured under the same experimental conditions and this over the course of 12 months. This interpretation is compatible with the cell surface fractionation assays showing that G449R was more likely to be found in the cell surface fraction than the WT channel complex in the presence of endogenous CaM, whereas this differential localization was not discernable when the cells

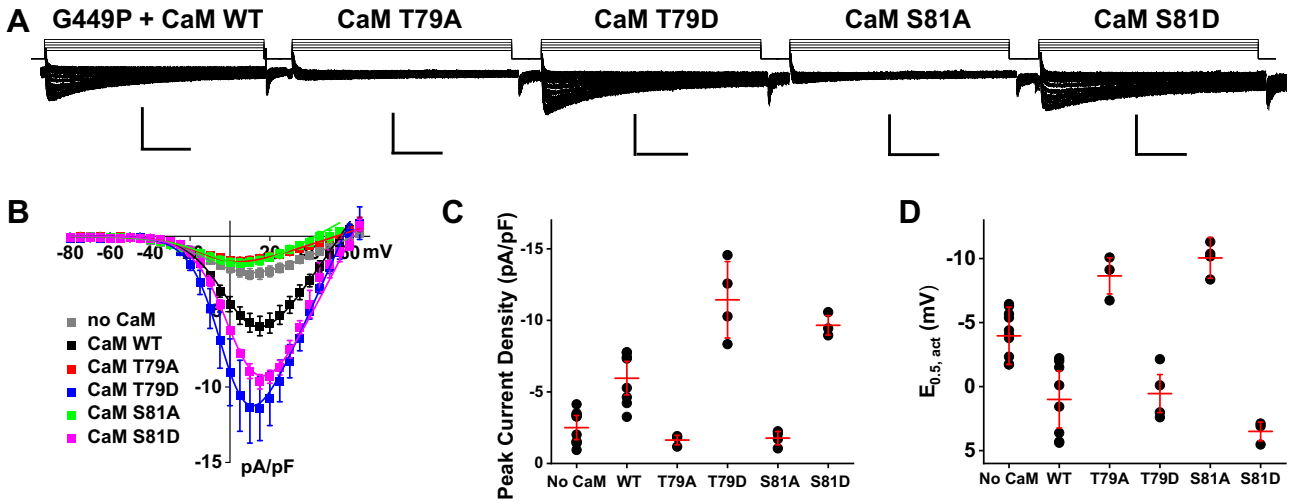

Figure 9. $Ca_V1.2$ G449P is modulated by CaM phosphorylation surrogates. *A*, whole-cell currents were recorded from HEKT cells transiently transfected with $Ca_V1.2$ G449P coexpressed with $Ca_V\beta2a$ and $Ca_V\alpha2\delta1$ and either CaM WT, with the phosphoresistant CaM (T79A or S81A), or with phosphomimetic CaM (T79D or S81D) as indicated. Exemplar traces are shown (from *left* to *right*) for $Ca_V1.2$ G449P + CaM WT, G449P + CaM T79A, G449P + CaM T79D, G449P + CaM S81A, and G449P + CaM S81D. The *vertical scale bars* are 10 pA/pF, and the *horizontal scale bars* are 100 ms throughout. *B*, the corresponding peak current densities are plotted as a function of applied voltage. *C* and *D*, the summarized distribution of the peak current densities and the midpotential of activation $E_{0.5,act}$. Peak whole-cell currents and $E_{0.5,act}$ are reported individually as *black circles*. The mean data ± SD are shown as *red hyphens*. Values of peak current densities and $E_{0.5,act}$ are reported in Table 6. CaM, calmodulin; HEKT, human embryonic kidney 293T cell line.

were saturated with overexpressed CaM. CaM bound to the C-terminal region of $Ca_V1.2$ has been previously reported to interact in a Ca^{2+}-dependent manner with the cytosolic I–II loop, where is located the glycine to arginine variant (70). It is thus conceivable that the higher "intrinsic" activity of G449R results from a stronger interaction with endogenous CaM. In this model, the cellular availability of CaM could modulate the operating window of $Ca_V1.2$.

$Ca_V1.2$ G449R is located in a structural region involved in activation gating (72), inactivation kinetics (73), protein stability, ubiquitination (74), and cell surface trafficking (75). The proximal segment of the first intracellular linker hosts the high-affinity binding site for $Ca_V\beta$ (76) and plays a role in networking with direct partners such as galectin (74) or Ras/Rad proteins through $Ca_V\beta$ (30, 77, 78). Glycine residues are unique in their lack of side-chain steric interference, permitting a higher flexibility to protein structures. Increasing flexibility by inserting glycine residues (29, 30) decreases channel function. In contrast, decreasing flexibility of this region by removing glycine residues promoted channel function (28, 31, 79, 80). The presence of a glycine residue proximal to the α-interacting domain in $Ca_V1.2$ WT could thus explain the requirement of a stronger depolarization in $Ca_V1.2$ WT *versus* G449R channels. The same position is already occupied by an arginine residue in $Ca_V2.2$ (31) and $Ca_V2.3$ channels whose activation is left shifted when compared with $Ca_V1.2$ under the same expression conditions (81).

The high-affinity binding site of $Ca_V\beta$ adopts an α-helical structure *in vitro* (82). The relative rigidity α-helix could promote a strong van der Waals interaction between the guanylate domain of $Ca_V\beta$ and hydrophobic residues of $Ca_V1.2$ (29, 83, 84). In the native protein, this α-helix breaks at the glycine located at position 449 (79). Crystallographic and circular dichroism spectroscopic studies demonstrated that the arginine substitution prolongs the α-helix (31). We also report that substitution with other α-helix-promoting residues, such as alanine (85), produced channels with strong activation properties, and from the contrary, substitution with proline, regarded as a α-helix breaker, was found to curb channel activation. The substituted channels however manifested distinct electrophysiological signatures in the presence of the phosphomimetic and phosphoresistant CaM proteins, from a complete indifference (G449K) to impaired peak current density in the presence of phosphoresistant CaM variants (G449A, G449D, G449P, and G449Q). Our data are compatible with the proposition that the longer α-helix enhances the coupling of the I–II linker with the inner pore responsible for channel activation. The intracellular linker would contribute to electromechanical coupling in $Ca_V1.2$ either through its intrinsic structural properties or following interaction with CaM.

The structural properties of the clinical variant could be envisioned to facilitate the interplay between accessory CaM proteins bound onto the C terminus of $Ca_V1.2$ and channel function as it was postulated for AKAP150 (86). In this context, the LQTS phenotype associated with the glycine to arginine substitution in the I–II linker could result from either process: an intrinsically stronger activation of $Ca_V1.2$ that renders the channel insensitive to cellular variations in phosphorylated CaM or else a higher affinity to CaM that causes the channel to be maximally activated at near endogenous concentration of CaM.

Experimental procedures

Recombinant DNA techniques

The $Ca_V\alpha1C$ subunit of $Ca_V1.2$ (GenBank accession number: X15539), $Ca_V\beta2a$ (GenBank accession number: NM_001398773), and $Ca_V\alpha2\delta1$ (GenBank accession number:

NM_000722) was subcloned in commercial vectors under the control of the cytomegalovirus (CMV) promoter as described elsewhere (36, 37, 75, 87). The cDNA sequence of the rabbit clone is near identical to the human clone save for an additional 30 amino acids in its N terminus, accounting for the +30 residue shift in residue numbering. The human CaM (GenBank accession number: M27319), subcloned in pcDNA3.1 (Thermo Fisher Scientific) vector with consecutive histidine (His-His-His-His-His-His) and cMyc (Glu-Gln-Lys-Leu-Iso-Ser-Glu-Glu-Asp-Leu) tags in C-terminal region, was a gift from Dr Rémy Sauvé, Université de Montréal. The cDNA mutations of CaM were introduced in this vector. CaM is numbered as reported (88) to take into account that the mature protein lacks N-terminal Met residue. All cDNA mutations in $Ca_V\alpha1C$ of $Ca_V1.2$ and CaM were produced with the Q5 Site-Directed Mutagenesis Kit (New England Biolabs, Inc) according to the manufacturer's instructions. Briefly, substitutions of nucleotides were created by incorporating the desired mutation in the center of the forward primer, and the reverse primer is designed so that the 5′ ends of the two primers anneal back to back. Following the PCR, the amplified DNA is circularized, and the template is removed with a kinase–ligase–DpnI enzyme mixture, before transformation into high-efficiency NEB DH5-α competent *Escherichia coli*. All constructs were verified by automated double-stranded sequence analysis ("Centre d'expertise et de services Génome Québec"). The protein expression at the expected molecular weight was confirmed by standard Western blot analysis for each construct.

Gene transfection and cell culture

HEKT cells were grown using standard tissue culture conditions (5% CO_2, 37 °C) in high-glucose Dulbecco's modified Eagle's medium supplemented with fetal bovine serum (10%), L-glutamine (2 mM), penicillin (100 U/ml), and streptomycin (10 mg/ml) as described before (36, 37, 75). Using Lipofectamine 2000 (Invitrogen), as per the manufacturer's instructions, HEKT cells (80% confluence, 35 mm petri dish) were transiently transfected with cDNA plasmids, namely pCMV-$Ca_V1.2$ WT or variants (4 μg), pCMV-$Ca_V\beta2a$ (4 μg), pCMV-$Ca_V\alpha2\delta1$ (4 μg), and in some experiments, pcDNA3-HisB-cMyc-CaM WT or variants (2 μg), with a weight ratio of 1:1:1:0.5 for a total of 12 to 14 μg cDNAs. The molar ratio was 7:1 for CaM and $Ca_V1.2$. Unless otherwise noted, the plasmids pCMV-$Ca_V\beta2a$, pCMV-$Ca_V\alpha2\delta1$, and pcDNA3-HisB-cMyc-CaM WT are simply referred to as $Ca_V\beta2a$, $Ca_V\alpha2\delta1$, and CaM WT in the text and figures. cDNA coding for peGFP (0.2 μg) was included in the cDNA mixture as a marker of successful transfection for patch-clamp experiments (4, 81). The culture medium was changed, and cells were detached with 0.05% trypsin before being replated on 35 mm petri dishes 6 h post-transfection. Whole-cell patch clamp experiments were performed 24 to 32 h after transfection.

Coimmunoprecipitation

HEKT cells were transiently transfected with the appropriate constructs (as indicated later), and protein extraction proceeded 2 days after transfection. Experiments described in Figure 2 were carried out as follows. HEKT cells were transiently transfected with $Ca_V1.2$ WT or $Ca_V1.2$ G449R with pCMV-$Ca_V\alpha2\delta1$ and cMyc-tagged versions of $Ca_V\beta3$ or $Ca_V\beta2a$ using, respectively, the pCMV-Tag5-$Ca_V\beta3$ or the pCMV-Tag5-$Ca_V\beta2a$ plasmids. $Ca_V\beta$ acted as the bait. Cell lysates were immunoprecipitated overnight with anti-cMyc magnetic beads (Pierce Anti-c-Myc Magnetic Beads; catalog no.: 88842, Thermo Fisher Scientific) to capture the given $Ca_V\beta$. In the experiments shown in Figures 4 and 5, the constructs were pCMV-$Ca_V\beta2a$ with pCMV-$Ca_V1.2$ WT or G449R and pcDNA3-HisB-cMyc-CaM WT and used CaM as the bait. Cell lysates were immunoprecipitated overnight with anti-His magnetic beads (code no.: MBL-D29111). The procedure was otherwise similar for the three experimental groups. Two different detergents have been used to compare extraction efficiency between digitonin (a nonionic saponin detergent) and CHAPS–Na (zwitterionic detergent). Both extraction conditions have produced the same results and were thus combined, for three independent experiments over the course of 2 months. Two days after transfection, cells were homogenized in 20 mM Na–Mops (pH 7.4), 300 mM NaCl, and 1% digitonin or 0.5% CHAPS–Na, supplemented with protease inhibitors without EDTA (Thermo Fisher Scientific). Homogenates were sonicated, incubated for 1 h at 4 °C, and centrifuged at 13,000 rpm for 30 min. A fraction (20 μg) of the homogenates or starting material was set aside as representative of total proteins and was immunoblotted to confirm normal protein expression. Coimmunoprecipitation was carried out using 200 μg homogenates diluted in 150 μl of 20 mM Na–Mops (pH 7.4) and 300 mM NaCl. The 200 ± 20 μl protein solution was incubated overnight with the appropriate antibody-coated magnetic beads that were collected using a PureProteome magnetic rack (Millipore). The magnetic beads were washed three times with a buffer containing 20 mM Na–Mops (pH 7.4), 300 mM NaCl, and 0.2% digitonin or alternatively 20 mM Na–Mops (pH 7.4), 300 mM NaCl, without additional detergent for the extraction under the "CHAPS conditions." The bound proteins were eluted with Laemmli buffer (20 μl) at 95 °C for 5 min, electrophoresed on a 6% or 10% SDS-polyacrylamide gel, and transferred onto a nitrocellulose membrane for Western blotting. Antibodies are described in the figure legends. Signals were detected with the enhanced chemiluminescence substrate. Blots were visualized with the ChemiDoc Touch system (Bio-Rad). Molecular weights were estimated using Image Lab software, version 5.2 (Bio-Rad) by linear regression of standard molecular weight markers.

Cell surface fractionation assay

Four different protein fractions (total cell lysates, cytosolic, total membrane, and plasma membrane fractions) were prepared as explained before (4). Briefly, transfected HEKT cells cultured in 100 mm dishes were homogenized at 4 °C in a Tris-based solution containing a mixture of protease inhibitors (Sigma) at pH 7.4. The cell homogenate was aliquoted into

three tubes. After a 2 h incubation period at 4 °C with 1% (v/v) Triton X-100, the first tube was centrifuged at 10,000*g* for 10 min to remove cell debris, nuclei, and mitochondria. The supernatant was kept as the total protein fraction (whole-cell lysates). The second tube was centrifuged at 200,000*g* and 4 °C for 20 min. The supernatant is referred to as the cytosolic fraction. The pellet was resuspended in homogenizing buffer containing 1% (v/v) Triton X-100. After 30 min of incubation on ice, a second centrifugation was performed at 200,000*g*. The resulting supernatant is referred to as the total membrane protein fraction. The third tube was centrifuged at 10,000*g* for 10 min. The supernatant obtained was centrifuged at 200,000*g* and 4 °C for 20 min. The pellet was resuspended in the homogenizing buffer containing 0.6 M KCl. Subsequent centrifugations were performed at 200,000*g* and 4 °C for 20 min to wash out the KCl. The final pellet was resuspended in the homogenizing buffer and is considered to be enriched in plasma membrane proteins. Proteins (20 μg) were electrophoresed on a 10% SDS-polyacrylamide gel.

Whole-cell patch-clamp recordings and data analysis

Whole-cell Ca^{2+} currents from transfected HEKT cells were recorded using pCLAMP software 11.2 (Molecular Devices) and an Axopatch 200B amplifier (Molecular Devices). Patch electrodes were pulled from borosilicate glass (Corning; code: 8161) and heat-polished to a final resistance about 3.0 to 3.5 MΩ when filled with the intracellular solution. Whole-cell currents were low-pass filtered at 2 kHz, digitized at a sampling rate of 100 μs during acquisition, and stored on a microcomputer equipped with an AD converter (Axon Digidata 1440A; Molecular Devices). Electrodes were filled with a solution containing (in millimolar) 140 CsCl, 0.6 NaGTP, 3 MgATP, 10 EGTA, 10 Hepes, titrated to pH 7.4 with NaOH. HEKT cells were bathed in a modified Earle's saline solution (in millimolar) as follows: 135 NaCl, 20 tetraethylammonium chloride, 2 $CaCl_2$, 1 $MgCl_2$, 10 Hepes, titrated to pH 7.4 with potassium hydroxide. Stock solution of the cell-permeable CaM antagonists W-13 *N*-(4-aminobutyl)-5-chloro-2-naphthalenesulfonamide and monohydrochloride (Tocris, Bio-Techne) was prepared in distilled water, diluted to its final concentration just before use, and added directly in the bath solution. Cells were incubated for 15 min prior to whole-cell recordings. A few experiments were performed in the presence of 2.5 μM TBB, a cell-permeable inhibitor of CK2. Stock solution of TBB (5 mM) was prepared in dimethylsulfoxide, diluted to its final concentration just before use, and added directly in the bath solution. Whole-cell currents were recorded 15 min after drug equilibration. All experiments were carried out at room temperature (23–25 °C). Cellular capacitance was estimated by measuring the time constant of current decay evoked by a depolarizing pulse pf 10 mV applied to the cell from a holding potential of −100 mV.

Whole-cell Ca^{2+} currents were elicited from a holding potential of −100 mV and depolarized to potentials ranging from −80 to 65 mV in 5 mV increments lasting 450 ms for each step. Ca^{2+} current densities (pA/pF) were obtained by dividing the peak current by the cell capacitance. Average *I–V* curves were obtained by plotting the peak current densities *versus* the voltage and fitted to a BoltzIV equation, which is a transformed Boltzmann function for *I–V* data of the following form:

$$I = \frac{(V_m - V_{rev}).G_{\max}}{1 + e^{(V - E_{0.5,act})/dx}}$$

where I is the current, V_m is the applied voltage, $E_{0.5,act}$ is the voltage at which channels are half-maximally activated, dx is the steepness of the slope, $G_{\max}$ is the maximal conductance, and V_{rev} is the reversal potential. Steady-state activation curves were constructed by dividing the peak I–V data by the driving force. The R100 ratio of $Ca_V1.2$ current was defined as the peak current remaining after a 100 ms depolarizing pulse (I_{100ms}/I_{peak}) and was used as an indicator of the inactivation kinetics. n/N refers to the number of cells/transfections measured in each condition of study.

The steady-state inactivation was determined using a two-step protocol in which conditioning prepulses were applied from a holding potential of −100 mV to a range of potentials from −100 to 40 mV in 10 mV increments for 5 s, immediately followed by a test pulse to 5 mV for 100 ms. For the construction of inactivation curves, the peak current amplitudes during the test pulses were normalized to the maximum peak current amplitude measured at −100 mV and plotted against the conditioning pulse. Steady-state inactivation curves were fitted to a modified Boltzmann equation:

$$I / I_{\max} = \frac{A1 - A2}{1 + e^{(V - E_{0.5,inact})/dx}} + A2$$

where $I/I_{\max}$ is the relative current measured at the test pulse, A1 and A2 represent, respectively, the maximum relative current value and the fraction of the noninactivated current, V_m is the voltage applied during the conditioning pulse, $E_{0.5,inact}$ is the voltage at which channels are half-maximally inactivated, and dx is the steepness of the slope.

Data analysis and statistics

Data were analyzed using a combination of pCLAMP software 11.2, Microsoft Excel, and OriginPro 2020 (OriginLab Corporation). Data in the tables are expressed as mean ± SD. Statistical significance was determined by one-way ANOVA and Bonferroni post hoc test in OriginPro 2020. The level of statistical significance was set at $p < 0.05$.

Data availability

All data are contained within the article.

Supporting information—This article contains supporting information.

Acknowledgments—We are grateful for the ongoing collaboration with Dr Rafik Tadros from the Cardiovascular Genetics Center at

the Montreal Heart Institute, and we thank Dr Rémy Sauvé for stimulating discussions and critical reading of the article.

Author contributions—L. P. conceptualization; J. Z., E. S., M. M., and L. P. methodology; J. Z., and L. P. validation; J. Z., and E. S. formal analysis; J. Z., E. S., and M. M. investigation; J. Z, E. S., and L. P. writing–original draft; L. P. supervision; L. P. project administration; L. P. funding acquisition; J. Z., E. S., M. M., and L. P. writing–review & editing.

Funding and additional information—This work was completed with the operating grant 159556 from the Canadian Institutes of Health Research to L.P. E.S. is the recipient of a PhD award from "Fonds de la recherche du Québec en nature et technologies."

Conflict of interest—The authors declare that they have no conflicts of interest with the contents of this article.

Abbreviations—The abbreviations used are: CaM, calmodulin; CDI, Ca^{2+}-dependent inactivation; cDNA, complementary DNA; CK2, casein kinase II; CMV, cytomegalovirus; HEK, human embryonic kidney cell line; LQTS, long-QT syndrome; TBB, 4,5,6,7-tetrabromobenzotriazole; TS, Timothy syndrome.

References

1. Grant, A. O. (2009) Cardiac ion channels. *Circ. Arrhythm. Electrophysiol.* **2**, 185–194
2. Wang, S. Q., Song, L. S., Lakatta, E. G., and Cheng, H. (2001) Ca2+ signalling between single L-type Ca2+ channels and ryanodine receptors in heart cells. *Nature* **410**, 592–596
3. Wu, J., Yan, Z., Li, Z., Qian, X., Lu, S., Dong, M., *et al.* (2016) Structure of the voltage-gated calcium channel Cav1.1 at 3.6 Å resolution. *Nature* **537**, 191–196
4. Segura, E., Bourdin, B., Tétreault, M. P., Briot, J., Allen, B. G., Mayer, G., *et al.* (2017) Proteolytic cleavage of the hydrophobic domain in the Ca(V)α2δ1 subunit improves assembly and activity of cardiac Ca(V)1.2 channels. *J. Biol. Chem.* **292**, 11109–11124
5. Colecraft, H. M., Alseikhan, B., Takahashi, S. X., Chaudhuri, D., Mittman, S., Yegnasubramanian, V., *et al.* (2002) Novel functional properties of Ca(2+) channel beta subunits revealed by their expression in adult rat heart cells. *J. Physiol.* **541**, 435–452
6. Van Petegem, F., Duderstadt, K. E., Clark, K. A., Wang, M., and Minor, D. L., Jr. (2008) Alanine-scanning mutagenesis defines a conserved energetic hotspot in the CaValpha1 AID-CaVbeta interaction site that is critical for channel modulation. *Structure* **16**, 280–294
7. Adams, P. J., Ben-Johny, M., Dick, I. E., Inoue, T., and Yue, D. T. (2014) Apocalmodulin itself promotes ion channel opening and Ca(2+) regulation. *Cell* **159**, 608–622
8. Zühlke, R. D., Pitt, G. S., Deisseroth, K., Tsien, R. W., and Reuter, H. (1999) Calmodulin supports both inactivation and facilitation of L-type calcium channels. *Nature* **399**, 159–162
9. Zühlke, R. D., Pitt, G. S., Tsien, R. W., and Reuter, H. (2000) Ca2+-sensitive inactivation and facilitation of L-type Ca2+ channels both depend on specific amino acid residues in a consensus calmodulin-binding motif in the(alpha)1C subunit. *J. Biol. Chem.* **275**, 21121–21129
10. Pate, P., Mochca-Morales, J., Wu, Y., Zhang, J. Z., Rodney, G. G., Serysheva, I. I., *et al.* (2000) Determinants for calmodulin binding on voltage-dependent Ca2+ channels. *J. Biol. Chem.* **275**, 39786–39792
11. Romanin, C., Gamsjaeger, R., Kahr, H., Schaufler, D., Carlson, O., Abernethy, D. R., *et al.* (2000) Ca(2+) sensors of L-type Ca(2+) channel. *FEBS Lett.* **487**, 301–306
12. Pitt, G. S., Zühlke, R. D., Hudmon, A., Schulman, H., Reuter, H., and Tsien, R. W. (2001) Molecular basis of calmodulin tethering and Ca2+-dependent inactivation of L-type Ca2+ channels. *J. Biol. Chem.* **276**, 30794–30802
13. Mouton, J., Feltz, A., and Maulet, Y. (2001) Interactions of calmodulin with two peptides derived from the c-terminal cytoplasmic domain of the Ca(v)1.2 Ca2+ channel provide evidence for a molecular switch involved in Ca2+-induced inactivation. *J. Biol. Chem.* **276**, 22359–22367
14. Jervell, A., and Lange-Nielsen, F. (1957) Congenital deaf-mutism, functional heart disease with prolongation of the Q-T interval and sudden death. *Am. Heart J.* **54**, 59–68
15. Liberthson, R. R. (1996) Sudden death from cardiac causes in children and young adults. *N. Engl. J. Med.* **334**, 1039–1044
16. Chugh, S. S., Reinier, K., Teodorescu, C., Evanado, A., Kehr, E., Al Samara, M., *et al.* (2008) Epidemiology of sudden cardiac death: clinical and research implications. *Prog. Cardiovasc. Dis.* **51**, 213–228
17. Schwartz, P. J., Stramba-Badiale, M., Crotti, L., Pedrazzini, M., Besana, A., Bosi, G., *et al.* (2009) Prevalence of the congenital long-QT syndrome. *Circulation* **120**, 1761–1767
18. Tester, D. J., and Ackerman, M. J. (2007) Postmortem long QT syndrome genetic testing for sudden unexplained death in the young. *J. Am. Coll. Cardiol.* **49**, 240–246
19. Tester, D. J., Will, M. L., Haglund, C. M., and Ackerman, M. J. (2005) Compendium of cardiac channel mutations in 541 consecutive unrelated patients referred for long QT syndrome genetic testing. *Heart Rhythm* **2**, 507–517
20. Splawski, I., Timothy, K. W., Sharpe, L. M., Decher, N., Kumar, P., Bloise, R., *et al.* (2004) Ca(V)1.2 calcium channel dysfunction causes a multisystem disorder including arrhythmia and autism. *Cell* **119**, 19–31
21. Splawski, I., Timothy, K. W., Decher, N., Kumar, P., Sachse, F. B., Beggs, A. H., *et al.* (2005) Severe arrhythmia disorder caused by cardiac L-type calcium channel mutations. *Proc. Natl. Acad. Sci. U. S. A.* **102**, 8089–8096. discussion 8086-8088
22. Gillis, J., Burashnikov, E., Antzelevitch, C., Blaser, S., Gross, G., Turner, L., *et al.* (2012) Long QT, syndactyly, joint contractures, stroke and novel CACNA1C mutation: Expanding the spectrum of Timothy syndrome. *Am. J. Med. Genet. A.* **158a**, 182–187
23. Po, C., Zordan, R., Vecchi, M., Cerutti, A., Sartori, S., Trevisson, E., *et al.* (2019) Photosensitive epilepsy and long QT: expanding Timothy syndrome phenotype. *Clin. Neurophysiol.* **130**, 2134–2136
24. Colson, C., Mittre, H., Busson, A., Leenhardt, A., Denjoy, I., Fressard, V., *et al.* (2019) Unusual clinical description of adult with Timothy syndrome, carrier of a new heterozygote mutation of CACNA1C. *Eur. J. Med. Genet.* **62**, 103648
25. Boczek, N. J., Ye, D., Jin, F., Tester, D. J., Huseby, A., Bos, J. M., *et al.* (2015) Identification and functional characterization of a novel CACNA1C-mediated cardiac disorder characterized by prolonged QT intervals with hypertrophic cardiomyopathy, congenital heart defects, and sudden cardiac death. *Circ. Arrhythm. Electrophysiol.* **8**, 1122–1132
26. Han, D., Xue, X., Yan, Y., and Li, G. (2019) Highlight article: dysfunctional Cav1.2 channel in Timothy syndrome, from cell to bedside. *Exp. Biol. Med. (Maywood)* **244**, 960–971
27. Hennessey, J. A., Boczek, N. J., Jiang, Y. H., Miller, J. D., Patrick, W., Pfeiffer, R., *et al.* (2014) A CACNA1C variant associated with reduced voltage-dependent inactivation, increased CaV1.2 channel window current, and arrhythmogenesis. *PLoS One* **9**, e106982
28. Kelu Bisabu, K., Zhao, J., Mokrane, A. E., Segura, É., Marsolais, M., Grondin, S., *et al.* (2020) Novel gain-of-function variant in CACNA1C associated with Timothy syndrome, multiple accessory pathways, and noncompaction cardiomyopathy. *Circ. Genom Precis Med.* **13**, e003123
29. Findeisen, F., and Minor, D. L., Jr. (2009) Disruption of the IS6-AID linker affects voltage-gated calcium channel inactivation and facilitation. *J. Gen. Physiol.* **133**, 327–343
30. Papa, A., Kushner, J., Hennessey, J. A., Katchman, A. N., Zakharov, S. I., Chen, B. X., *et al.* (2021) Adrenergic Ca(V)1.2 activation via Rad phosphorylation converges at α(1C) I-II loop. *Circ. Res.* **128**, 76–88
31. Almagor, L., Chomsky-Hecht, O., Ben-Mocha, A., Hendin-Barak, D., Dascal, N., and Hirsch, J. A. (2012) The role of a voltage-dependent Ca2+ channel intracellular linker: A structure-function analysis. *J. Neurosci.* **32**, 7602–7613
32. Barrett, C. F., and Tsien, R. W. (2008) The Timothy syndrome mutation differentially affects voltage- and calcium-dependent inactivation of

CaV1.2 L-type calcium channels. *Proc. Natl. Acad. Sci. U. S. A.* **105**, 2157–2162
33. Dick, I. E., Joshi-Mukherjee, R., Yang, W., and Yue, D. T. (2016) Arrhythmogenesis in Timothy Syndrome is associated with defects in Ca(2+)-dependent inactivation. *Nat. Commun.* **7**, 10370
34. Raybaud, A., Dodier, Y., Bissonnette, P., Simoes, M., Bichet, D. G., Sauvé, R., *et al.* (2006) The role of the GX9GX3G motif in the gating of high voltage-activated Ca2+ channels. *J. Biol. Chem.* **281**, 39424–39436
35. Tarnovskaya, S. I., Kostareva, A. A., and Zhorov, B. S. (2021) L-type calcium channel: predicting pathogenic/likely pathogenic status for variants of uncertain clinical significance. *Membranes* **11**, 599
36. Bourdin, B., Briot, J., Tétreault, M. P., Sauvé, R., and Parent, L. (2017) Negatively charged residues in the first extracellular loop of the L-type Ca(V)1.2 channel anchor the interaction with the Ca(V)α2δ1 auxiliary subunit. *J. Biol. Chem.* **292**, 17236–17249
37. Briot, J., Mailhot, O., Bourdin, B., Tétreault, M. P., Najmanovich, R., and Parent, L. (2018) A three-way inter-molecular network accounts for the Ca(V)α2δ1-induced functional modulation of the pore-forming Ca(V)1.2 subunit. *J. Biol. Chem.* **293**, 7176–7188
38. Saimi, Y., and Kung, C. (2002) Calmodulin as an ion channel subunit. *Annu. Rev. Physiol.* **64**, 289–311
39. Urrutia, J., Aguado, A., Muguruza-Montero, A., Núñez, E., Malo, C., Casis, O., *et al.* (2019) The crossroad of ion channels and calmodulin in disease. *Int. J. Mol. Sci.* **20**, 400
40. Tiaho, F., Piot, C., Nargeot, J., and Richard, S. (1994) Regulation of the frequency-dependent facilitation of L-type Ca2+ currents in rat ventricular myocytes. *J. Physiol.* **477**, 237–251
41. Villarroel, A., Taglialatela, M., Bernardo-Seisdedos, G., Alaimo, A., Agirre, J., Alberdi, A., *et al.* (2014) The ever changing moods of calmodulin: how structural plasticity entails transductional adaptability. *J. Mol. Biol.* **426**, 2717–2735
42. Persechini, A., and Stemmer, P. M. (2002) Calmodulin is a limiting factor in the cell. *Trends Cardiovasc. Med.* **12**, 32–37
43. DeMaria, C. D., Soong, T. W., Alseikhan, B. A., Alvania, R. S., and Yue, D. T. (2001) Calmodulin bifurcates the local Ca2+ signal that modulates P/Q-type Ca2+ channels. *Nature* **411**, 484–489
44. Simms, B. A., Souza, I. A., and Zamponi, G. W. (2014) Effect of the Brugada syndrome mutation A39V on calmodulin regulation of Cav1.2 channels. *Mol. Brain* **7**, 34
45. Ravindran, A., Lao, Q. Z., Harry, J. B., Abrahimi, P., Kobrinsky, E., and Soldatov, N. M. (2008) Calmodulin-dependent gating of Ca(v)1.2 calcium channels in the absence of Ca(v)beta subunits. *Proc. Natl. Acad. Sci. U. S. A.* **105**, 8154–8159
46. Limpitikul, W. B., Dick, I. E., Joshi-Mukherjee, R., Overgaard, M. T., George, A. L., Jr., and Yue, D. T. (2014) Calmodulin mutations associated with long QT syndrome prevent inactivation of cardiac L-type Ca(2+) currents and promote proarrhythmic behavior in ventricular myocytes. *J. Mol. Cell Cardiol.* **74**, 115–124
47. Nowycky, M. C., Fox, A. P., and Tsien, R. W. (1985) Long-opening mode of gating of neuronal calcium channels and its promotion by the dihydropyridine calcium agonist Bay K 8644. *Proc. Natl. Acad. Sci. U. S. A.* **82**, 2178–2182
48. Asmara, H., Minobe, E., Saud, Z. A., and Kameyama, M. (2010) Interactions of calmodulin with the multiple binding sites of Cav1.2 Ca2+ channels. *J. Pharmacol. Sci.* **112**, 397–404
49. Wang, H. G., George, M. S., Kim, J., Wang, C., and Pitt, G. S. (2007) Ca/Calmodulin regulates trafficking of Cav1.2 Ca channels in cultured hippocampal neurons. *J. Neurosci.* **27**, 9086–9093
50. Osawa, M., Swindells, M. B., Tanikawa, J., Tanaka, T., Mase, T., Furuya, T., *et al.* (1998) Solution structure of calmodulin-W-7 complex: the basis of diversity in molecular recognition. *J. Mol. Biol.* **276**, 165–176
51. Osawa, M., Kuwamoto, S., Izumi, Y., Yap, K. L., Ikura, M., Shibanuma, T., *et al.* (1999) Evidence for calmodulin inter-domain compaction in solution induced by W-7 binding. *FEBS Lett.* **442**, 173–177
52. Quadroni, M., James, P., and Carafoli, E. (1994) Isolation of phosphorylated calmodulin from rat liver and identification of the *in vivo* phosphorylation sites. *J. Biol. Chem.* **269**, 16116–16122
53. Villalobo, A. (2018) The multifunctional role of phospho-calmodulin in pathophysiological processes. *Biochem. J.* **475**, 4011–4023
54. Tabernero, L., Taylor, D. A., Chandross, R. J., VanBerkum, M. F., Means, A. R., Quiocho, F. A., *et al.* (1997) The structure of a calmodulin mutant with a deletion in the central helix: implications for molecular recognition and protein binding. *Structure* **5**, 613–622
55. Bildl, W., Strassmaier, T., Thurm, H., Andersen, J., Eble, S., Oliver, D., *et al.* (2004) Protein kinase CK2 is coassembled with small conductance Ca(2+)-activated K+ channels and regulates channel gating. *Neuron* **43**, 847–858
56. Plancke, Y. D., and Lazarides, E. (1983) Evidence for a phosphorylated form of calmodulin in chicken brain and muscle. *Mol. Cell Biol.* **3**, 1412–1420
57. Quadroni, M., L'Hostis, E. L., Corti, C., Myagkikh, I., Durussel, I., Cox, J., *et al.* (1998) Phosphorylation of calmodulin alters its potency as an activator of target enzymes. *Biochemistry* **37**, 6523–6532
58. Sacks, D. B., Davis, H. W., Crimmins, D. L., and McDonald, J. M. (1992) Insulin-stimulated phosphorylation of calmodulin. *Biochem. J.* **286**, 211–216
59. Sacks, D. B., Mazus, B., and Joyal, J. L. (1995) The activity of calmodulin is altered by phosphorylation: modulation of calmodulin function by the site of phosphate incorporation. *Biochem. J.* **312**, 197–204
60. Li, S. C., Goto, N. K., Williams, K. A., and Deber, C. M. (1996) Alpha-helical, but not beta-sheet, propensity of proline is determined by peptide environment. *Proc. Natl. Acad. Sci. U. S. A.* **93**, 6676–6681
61. Ambrosino, P., Alaimo, A., Bartollino, S., Manocchio, L., De Maria, M., Mosca, I., *et al.* (2015) Epilepsy-causing mutations in Kv7.2 C-terminus affect binding and functional modulation by calmodulin. *Biochim. Biophys. Acta* **1852**, 1856–1866
62. Ben-Johny, M., and Yue, D. T. (2014) Calmodulin regulation (calmodulation) of voltage-gated calcium channels. *J. Gen. Physiol.* **143**, 679
63. Kim, E. Y., Rumpf, C. H., Fujiwara, Y., Cooley, E. S., Van Petegem, F., and Minor, J. (2008) Structures of CaV2 Ca2+/CaM-IQ domain complexes reveal binding modes that underlie calcium-dependent inactivation and facilitation. *Structure* **16**, 1455–1467
64. Van Petegem, F., Chatelain, F. C., and Minor, D. L., Jr. (2005) Insights into voltage-gated calcium channel regulation from the structure of the CaV1.2 IQ domain-Ca2+/calmodulin complex. *Nat. Struct. Mol. Biol.* **12**, 1108–1115
65. Dick, I. E., Tadross, M. R., Liang, H., Tay, L. H., Yang, W., and Yue, D. T. (2008) A modular switch for spatial Ca2+ selectivity in the calmodulin regulation of CaV channels. *Nature* **451**, 830–834
66. Simms, B. A., Souza, I. A., and Zamponi, G. W. (2014) A novel calmodulin site in the Cav1.2 N-terminus regulates calcium-dependent inactivation. *Pflugers Arch.* **466**, 1793–1803
67. Ivanina, T., Blumenstein, Y., Shistik, E., Barzilai, R., and Dascal, N. (2000) Modulation of L-type Ca2+ channels by gbeta gamma and calmodulin via interactions with N and C termini of alpha 1C. *J. Biol. Chem.* **275**, 39846–39854
68. Noble, S., and Shimoni, Y. (1981) The calcium and frequency dependence of the slow inward current 'staircase' in frog atrium. *J. Physiol.* **310**, 57–75
69. Marban, E., and Tsien, R. W. (1982) Enhancement of calcium current during digitalis inotrophy in mammalian heart: positive feed-back regulation by intracellular calcium? *J. Physiol.* **329**, 589–614
70. Kim, J., Ghosh, S., Nunziato, D. A., and Pitt, G. S. (2004) Identification of the components controlling inactivation of voltage-gated Ca(2+) channels. *Neuron* **41**, 745–754
71. Campiglio, M., and Flucher, B. E. (2015) The role of auxiliary subunits for the functional diversity of voltage-gated calcium channels. *J. Cell Physiol.* **230**, 2019–2031
72. Beyl, S., Depil, K., Hohaus, A., Stary-Weinzinger, A., Timin, E., Shabbir, W., *et al.* (2011) Physicochemical properties of pore residues predict activation gating of CaV1.2: a correlation mutation analysis. *Pflugers Arch.* **461**, 53–63

73. Dafi, O., Berrou, L., Dodier, Y., Raybaud, A., Sauvé, R., and Parent, L. (2004) Negatively charged residues in the N-terminal of the AID helix confer slow voltage dependent inactivation gating to CaV1.2. *Biophys. J.* **87**, 3181–3192
74. Hu, Z., Li, G., Wang, J.-W., Chong, S. Y., Yu, D., Wang, X., *et al.* (2018) Regulation of blood pressure by targeting CaV1.2-galectin-1 protein interaction. *Circulation* **138**, 1431–1445
75. Bourdin, B., Marger, F., Wall-Lacelle, S., Schneider, T., Klein, H., Sauvé, R., *et al.* (2010) Molecular determinants of the CaVbeta-induced plasma membrane targeting of the CaV1.2 channel. *J. Biol. Chem.* **285**, 22853–22863
76. Buraei, Z., and Yang, J. (2010) The β subunit of voltage-gated Ca2+ channels. *Physiol. Rev.* **90**, 1461–1506
77. Finlin, B. S., Crump, S. M., Satin, J., and Andres, D. A. (2003) Regulation of voltage-gated calcium channel activity by the Rem and Rad GTPases. *Proc. Natl. Acad. Sci. U. S. A.* **100**, 14469–14474
78. Liu, G., Papa, A., Katchman, A. N., Zakharov, S. I., Roybal, D., Hennessey, J. A., *et al.* (2020) Mechanism of adrenergic CaV1.2 stimulation revealed by proximity proteomics. *Nature* **577**, 695–700
79. Almagor, L., Avinery, R., Hirsch, J. A., and Beck, R. (2013) Structural flexibility of CaV1.2 and CaV2.2 I-II proximal linker fragments in solution. *Biophys. J.* **104**, 2392–2400
80. Almagor, L., Chomsky-Hecht, O., Ben-Mocha, A., Hendin-Barak, D., Dascal, N., and Hirsch, J. A. (2012) CaV1.2 I-II linker structure and Timothy syndrome. *Channels (Austin)* **6**, 468–472
81. Shakeri, B., Bourdin, B., Demers-Giroux, P. O., Sauvé, R., and Parent, L. (2012) A quartet of leucine residues in the guanylate kinase domain of CaVβ determines the plasma membrane density of the CaV2.3 channel. *J. Biol. Chem.* **287**, 32835–32847
82. Opatowsky, Y., Chen, C. C., Campbell, K. P., and Hirsch, J. A. (2004) Structural analysis of the voltage-dependent calcium channel beta subunit functional core and its complex with the alpha 1 interaction domain. *Neuron* **42**, 387–399
83. Van Petegem, F., Clark, K. A., Chatelain, F. C., and Minor, D. L., Jr. (2004) Structure of a complex between a voltage-gated calcium channel beta-subunit and an alpha-subunit domain. *Nature* **429**, 671–675
84. Chen, Y. H., Li, M. H., Zhang, Y., He, L. L., Yamada, Y., Fitzmaurice, A., *et al.* (2004) Structural basis of the alpha1-beta subunit interaction of voltage-gated Ca2+ channels. *Nature* **429**, 675–680
85. Pace, N. C., and Scholtz, M. J. (1998) A helix propensity scale based on experimental studies of peptides and proteins. *Biophys. J.* **75**, 422–427
86. Dixon, R. E., Cheng, E. P., Mercado, J. L., and Santana, L. F. (2012) L-type Ca2+ channel function during Timothy syndrome. *Trends Cardiovasc. Med.* **22**, 72–76
87. Bourdin, B., Shakeri, B., Tétreault, M. P., Sauvé, R., Lesage, S., and Parent, L. (2015) Functional characterization of CaVα2β mutations associated with sudden cardiac death. *J. Biol. Chem.* **290**, 2854–2869
88. Lee, C. H., and MacKinnon, R. (2018) Activation mechanism of a human SK-calmodulin channel complex elucidated by cryo-EM structures. *Science* **360**, 508–513